CHALMERS

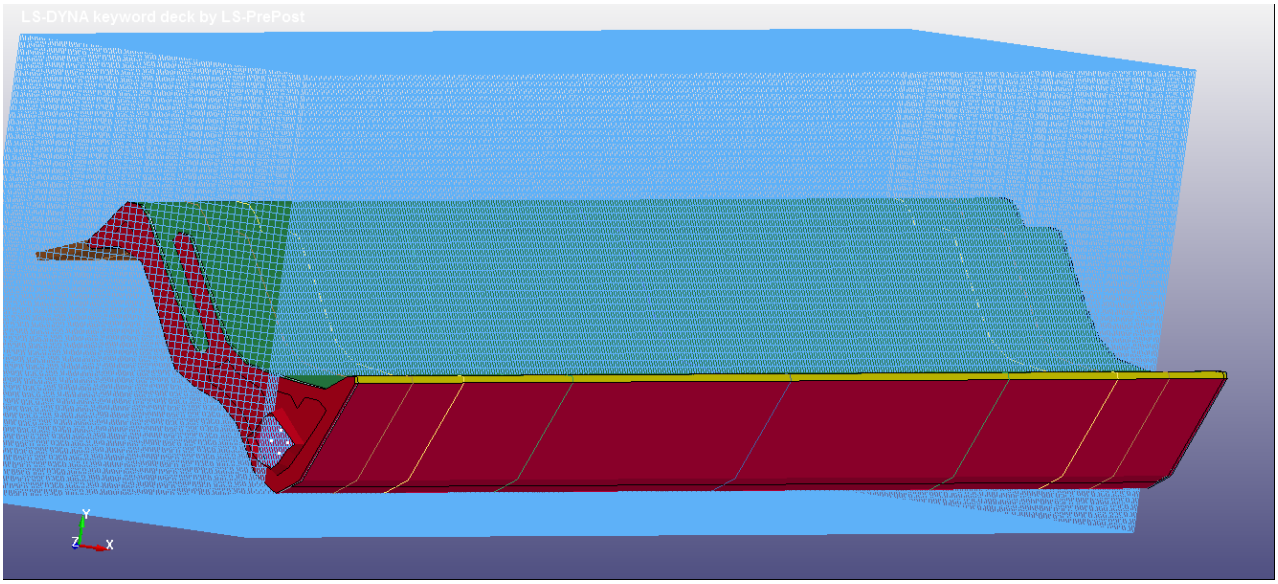

Expansion of a folded thin-walled sheet metal structure using a Novel Approach to Fluid Structure Interaction

Master's thesis in Applied Mechanics

CARL ONSJÖ

Department of Applied Mechanics
CHALMERS UNIVERSITY OF TECHNOLOGY
Göteborg, Sweden 2015

MASTER'S THESIS IN APPLIED MECHANICS

Expansion of a folded thin-walled sheet metal structure using a Novel Approach to Fluid Structure Interaction

CARL ONSJÖ

Department of Applied Mechanics
Division of Solid Mechanics
CHALMERS UNIVERSITY OF TECHNOLOGY

Göteborg, Sweden 2015

Expansion of a folded thin-walled sheet metal structure using a Novel Approach to Fluid Structure Interaction
CARL ONSJÖ

Master's thesis 2015:77
ISSN 1652-8557
Department of Applied Mechanics
Division of Solid Mechanics
Chalmers University of Technology
SE-412 96 Göteborg
Sweden
Telephone: +46 (0)31-772 1000

Cover:
Model of A-pillar in its original state and some of the hexagonal mesh of the computational domain

Chalmers Reproservice
Göteborg, Sweden 2015

Expansion of a folded thin-walled sheet metal structure using a Novel Approach to Fluid Structure Interaction
Master's thesis in Applied Mechanics
CARL ONSJÖ
Department of Applied Mechanics
Division of Solid Mechanics
Chalmers University of Technology

Abstract

The FE modeling of expandable thin-walled sheet metal components has been studied in this work. The key benefit of such adaptive (shape-changing) components is that they can be transformed from a close-packed state to an expanded state (supported by internal pressure) very rapidly in a safety critical situation.

A thin-walled component with significant potential for being made adaptive this way is the A-pillar of a car. The A-pillar is a pivotal component of the passive crash safety. However, making this component stiff and strong inherently also leads to an increase in dimensions (and weight) which in the end might have a negative influence on the overall crash safety since the visibility for the driver is reduced. Research efforts at Autoliv have been focused on developing a concept for an expanding A-pillar (by pressurization) in the event of a crash, keeping the initial dimensions (and weight) low, thereby maximizing the visibility for the driver, and still meeting the stiffness and strength requirements in a crash when expanded.

The implementation of such an adaptive concept in cars in series production relies on good predictability of the expansion process and subsequent deformation under loading in numerical crash simulation. This requires to be able to model and simulate the interaction between the flowing gas in the component and the walls of the same, which from a numerical point of view is very challenging, especially due to the high flow rates. Previous attempts made at Autoliv using a coupled Euler-Lagrange method to the structural solver in LS-DYNA has revealed significant gas leakage through the solid walls, whereby a new approach has been evaluated in the current project. Consequently, the simulation of the fluid part involved has been done using the newly developed Conservation Element/Solution Element (CESE) solver in LS-Dyna coupled to the structural solver in the same software.

A model of an expandable thin-walled sheet metal structure has been developed and assessed. The ultimate simulation model applied an immersed boundary approach to couple the fluid with the solid walls, using a hexagonal mesh for the fluid and boundary conditions specified at the surface of volume elements of the fluid domain. Other techniques have also been evaluated and documented e.g. the effectiveness of different meshing techniques.

The fluid motion solver was validated through benchmarking against Sod's shock tube and a case studying supersonic flow around a wedge shaped object. In the subsequent fluid-structure interaction case, the final model proved to have leakage issues making it difficult to assess whether the conversion from mass flow of the gas generator used in a previous project was successful, but a tank test was indicative of success. Expansion of a folded sheet metal structure (the A-pillar) was finally achieved by increasing inlet pressure to the highest amount the solver could handle (unrealistically high) to offset the adverse effects of leakage.

Keywords: LS-Dyna, CESE, FSI, FEM, CFD

Acknowledgements

First of all the author would like to thank everyone at the research department at Autoliv, Vårgårda for all the good times at lunches and breaks, secondly his supervisor Bengt Pipkorn at said company for teaching him the mantra of one step at a time, thirdly Marcus Timgren at Dynamore for all the excellent support and, lastly, he would like to extend his gratitude to the examiner and also supervisor at Chalmers, Martin Fagerström, who has been very helpful in making the work go more smoothly.

Carl Onsjö, Gothenburg November 9, 2015

Contents

1 Introduction

1.1 Background

The study of thin-walled structures have many application areas. Many safety features rely on the structural integrity that can be achieved by arranging sheet metal into different geometric shapes that have vastly different engineering properties. The key point is that weight efficient components that are both strong and stiff may be designed as members with (large) hollow cross sections with a small wall thickness. Interestingly, such thin-walled components can be made adaptive such that, in the original state the component is folded. Then, if needed, the component may be expanded (e.g. via internal gas pressure) to a shape which has much higher structural performance. This way, space can be saved in the original design.

A thin-walled component with significant potential for being made adaptive this way is the A-pillar of a car. The A-pillar is a pivotal component of the passive crash safety. However, making this component stiff and strong inherently also leads to an increase in dimensions (and weight) which in the end might have a negative influence on the overall crash safety since the visibility for the driver is reduced. Thus, visibility and structural integrity are, using non-adaptive techniques, mutually exclusive requirements because of the inherent bulkiness of a crash-resistant frame Therefore, research efforts at Autoliv have been spent on developing a concept for an expanding A-pillar (by pressurization using a gas generator) in the event of a crash, keeping the initial dimensions (and weight) low, thereby maximizing the visibility for the driver, and still meeting the stiffness and strength requirements in a crash when expanded. Experiments have been done using steel constructions and the results have shown that further investigations are worthwhile. The results have been written about in automotive magazines, e.g. Figure 1.1 from Car and driver.

Absolutely crucial for the implementation of such an adaptive concept in cars in series production is however to have a good predictability of the expansion process and subsequent deformation under loading in numerical crash simulation. This requires to be able to model and simulate the interaction between the flowing gas in the component and the walls of the same, so-called Fluid structure interaction (FSI), which from a numerical point of view is very challenging, especially due to the high flow rates. Structural analysis of folded thin-walled sheet metal structures is nothing new, but if expansion of a folded structure is desired then FSI will be needed.

FSI is a multi-physics science which combines computational fluid dynamics with structural mechanics calculations. Traditionally FSI has been used to predict the effects of fatigue in materials in order to prevent disasters such as the failure of Tacoma Bridge in 1940 [1]. In this project nothing of that magnitude was studied, but the methods are alike all the same. Previous attempts to simulate the expansion made at Autoliv using a coupled Euler-Lagrange method to the structural solver in LS-DYNA has revealed significant gas leakage through the solid walls and inconclusive results [2], whereby a new approach has been evaluated in the current project. Consequently, the simulation of the fluid part involved has been done using the newly developed Conservation Element/Solution Element (CESE) solver in LS-Dyna coupled to the structural solver in the same software.

In this project the software LS-DYNA which is a combined implicit/explicit solver for highly non-linear, transient problems within multi-physics and multi-stage applications has been used. LS-DYNA is widely used for multi physics applications and therefore a vital tool in this analysis.

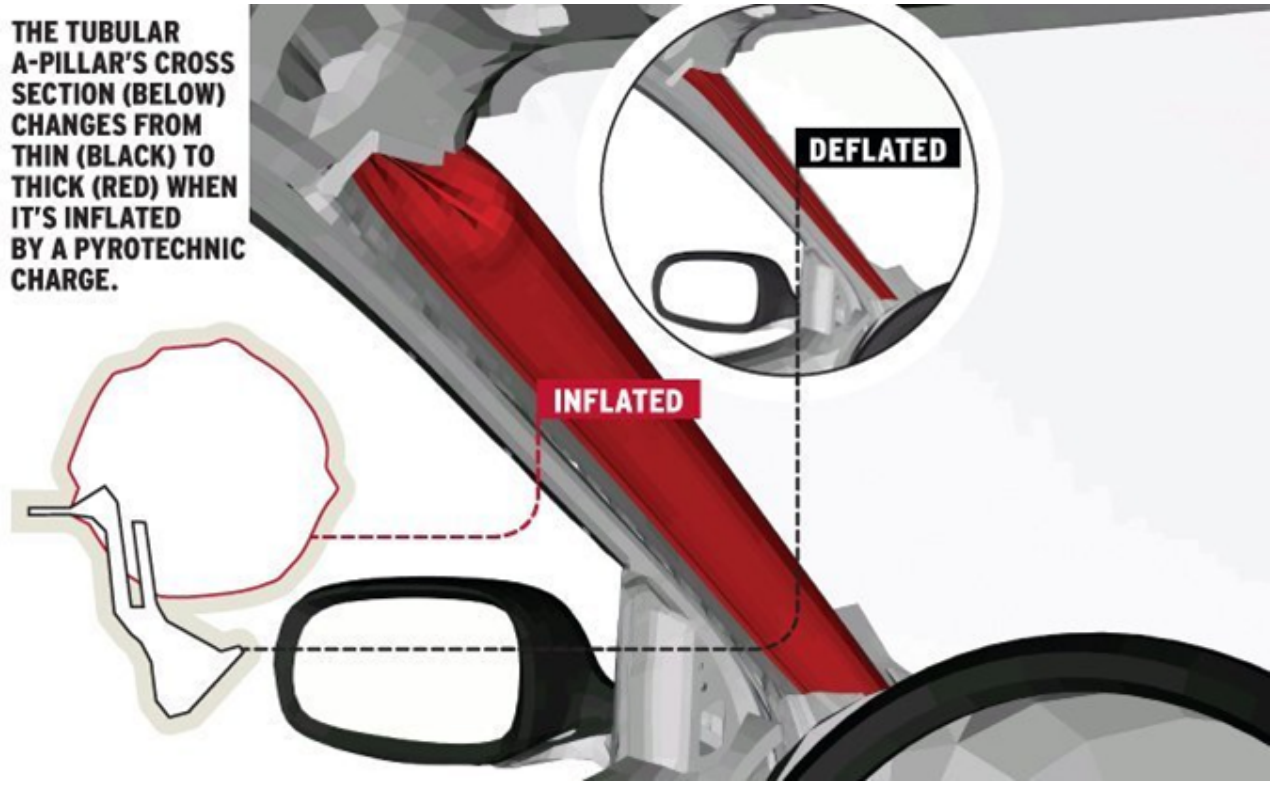

Figure 1.1: *Position of A-pillar in a car. Figure taken from:* www.caranddriver.com

Livermore Software

Technology Corporation (LSTC, creators of LS-DYNA) has recently developed a new type of Navier-Stokes solver for compressible flow applications, and this is virtually untested on this type of problem, and that's why this project is of academic interest as well as industrially significant. Because of the recent developments by LSTC regarding FSI it is viable to apply their newly created tools to this specific problem.

1.2 Aim

The aim of this project has been to evaluate an improved method for analysing the expansion av a folded thin-walled sheet metal structure using the new conservation element/solution element (CESE) method coupled to a mechanical structure solver with fluid structure interaction.

More specifically the following goals have been defined:

- Verify the CESE solver
- Ascertain which fluid phenomena was present in the final simulation
- Develop a workflow for simulation of fluid structure interaction using the CESE solver
- Evaluate the results from the simulated expansion of an A-pillar
- Make a list of recommendations for simulating cases of this sort

1.3 Limitations

A comparison between numerical results and physical results is not made since there are analytical solutions available during the verification stage of the project. Only the CESE solver is used to simulate the flow, even though the boundary condition set up is not as accurate when defining the mass flow as previous simulation models have been. Only one gas can be simulated as the propulsion of the expansion unlike the previous model, which applies a corpuscular particle solver and can accomodate a mixture of gases instead. The theory behind the numerical scheme used in the solver will not be explained in detail as this is not needed for this industrial application.

1.4 Approach

The solver was first evaluated using two tests which could be compared to analytical solutions. The first test was Sod's shock tube, a standard benchmark to run on solvers made for compressible flow. A second test in which a simulation of a wedge experiment designed to test how well the solver predicts oblique shock waves and expansion fans (areas of incremental pressure drop) in 2D was done, and finally the data from a previous simulation of a gas generator had to be adapted to boundary conditions applicable to the CESE solver, before the expansion of the A-pillar could be simulated using the derived boundary conditions. During the project several boundary methods and meshing setups were tried and evaluated.

2 Theory

In this chapter the reader will find the theoretical background needed to perform the analysis in the thesis. First of all the basic theory on fluid dynamics is presented, covering what needs to be understood for seperating incompressible flow from compressible. Secondly, the discretization scheme used in the software to perform the analysis of the problems described in this report will be explained. Finally a description on how the fluid analysis solver and the structure analysis is coupled in the aforementioned software will follow.

2.1 Governing Equations for Fluid Dynamics

The three-dimensional Navier-Stokes equation and the effects stemming from compressibility of a fluid. Expressed using the Einstein summation notation, $i = 1,2,3$.

2.1.1 Three-dimensional, incompressible Navier-Stokes

The equations for three-dimensional flow were named after Claude-Louis Navier and George Gabriel Stokes. The equations were derived from Newton's second law applied to the motion of fluids. The general case is that of viscous flow, where the stress apparent in the fluid is described by the sum of a diffusing viscous term that in itself is proportional to the gradient of the flow velocity. [3]

The Navier-Stokes' equations are as follows [4] (using Einstein summation convention).

The mass continuity equation: This equation is known as the mass continuity equation and is derived from the conservation of mass in a control volume. It states that

$$\dot{\rho} + \rho v_{i,i} = 0 \tag{2.1}$$

where $\dot{\rho}$ = density change over time, ρ = density and $v_{i,i}$ is the spatial derivative of the flow field.

The compressible Navier-Stokes equations: The compressible Navier-Stokes equations are derived from the constitutive law for Newtonian viscous fluids and are as follows:

$$\frac{\partial(\rho v_i)}{\partial t} + \frac{\partial[\rho v_i v_j]}{\partial x_j} = -\frac{\partial p}{\partial x_i} + \frac{\partial \tau_{ij}}{\partial x_j} + \rho f_i \tag{2.2}$$

where ρ=density, t=time, v_i=velocity tensor component, x_i=coordinate direction, p=pressure, τ_{ij}=viscous stress tensor, f_i=external forces.

This equation becomes non-linear when the flow speed surpasses Mach 0.33 [4] and becomes compressible as $\rho = \rho(x_i)$ in that case.

The energy equation: With u=internal energy, q_i=conductive heat flux, and z=the net radiative heat source

$$\rho\frac{\partial u}{\partial t} - v_{i,j}\sigma_{ji} + q_{i,i} = \rho z \tag{2.3}$$

where

$$\sigma_{ij} = -p\delta_{ij} + 2\mu S_{ij} - \frac{2}{3}\mu S_{kk}\delta_{ij} \tag{2.4}$$

δ_{ij} denotes the Croenecker delta, S_{ij} is the strain-rate tensor

The three equations (2.1, 2.2 and 2.3) above are what is needed to solve all state variables for fluid motion.

2.2 Effects in compressible flow

Within compressible flow there are other effects apparent than those in the case of low fluid velocity. Large discontinuities in pressure, flow speed, density and temperature will be visible [5]. These discontinuities will manifest themselves in different ways such as Mach waves, reflection waves, expansion fans, etc. [6] and will affect the flow propagation. It is important to have a solver that is capable of resolving these discontinuities and thereby factoring them in to the next iteration so as to achieve solutions of high accuracy.

2.3 Conservation Element/Solution Element method

The space-time conservation element and solution element (CESE) is a new numerical framework for solving conservation laws in continuum mechanics. It was developed to provide robustness, generality, simplicity and accuracy. This method has showed great results for shock tube problems, the ZND detonation waves (model of explosives), the implosion and explosion problem, shocks over a forward-facing step, the blast wave issuing from a nozzle, various

acoustic waves, and shock/acoustic wave interactions to name a few [7]. A one dimensional example can be found in [8].

This high performance when it comes to compressible flow, and the effects thereof, makes the CESE method a likely candidate to handle the expansion of a folded thin-walled sheet metal structure. As the stringent mathematical explanation would be outside the scope of this thesis only an explanation of the main features of the CESE method is given.

Both space and time are treated in the same way. Each Solution Element (SE) consist of the discretized space-time domain and contains a simple (linear, for example) function of space and time. Conservation Elements (CE) fill the space-time domain without overlap to bind the SEs together and the points on each face of a CE is attached to a single SE.

Whereas traditional methods only address spatial flux conservation the CESE method solves the integral form of the conservation law in the space-time domain. This and two other features guarantee that the flux is conserved in both space and time: the CEs fill space-time without overlap and the flux through any face of a CE is uniquely defined. The CESE method does not make any assumptions on the solution before it is derived, i.e. characteristics or shock-wave profiles, and can therefore be viewed as completely general.

The employed space-time mesh is staggered (evaluating different scalar variables at different places) to evaluate the inviscid flux information at the separating interface between two CEs completely without interpolation or extrapolation. The CESE method can be used to construct explicit solvers that are non-dissipative for CFL numbers below one for isentropic and inviscid flows.

2.3.1 Stabilization methods in LS-DYNA

The method described above and in the example in [8] is stable for inviscid flow with no discontinuities, i.e. shock waves. As this is not enough for most problems concerning compressible flow it is necessary to introduce some numerical diffusive stabilization. This is done by using a combination of the flow speeds at the faces of the solution elements at the previous time-step and comparing them to the exact solution in the current time-step. Thus only one CE has to be used since there is only one unknown per flow direction. More information on this can be found in the theory manual for the CESE solver [9].

2.4 Governing Equations for Solid Mechanics

The theory behind the structure mechanics solver in LS-DYNA is completely explained in their theory manual [10], and the reader is referred here for a complete explanation. A short explanation can be found below.

The mechanics solver in LS-DYNA seeks the solution to the momentum equation

$$\sigma_{ij,j} + \rho f_i = \rho \ddot{x}_i \tag{2.5}$$

with a traction boundary condition and other applicable boundary conditions. $\sigma_{ij,j}$ is the divergence of the Cauchy stress tensor, ρ is the current density, f is the body force density, $\ddot{x}_i$ is the acceleration with the comma denoting covariant differentiation, n_j is a unit outward normal.

Mass is conserved as $\rho V = \rho_0$ with V as the relative volume as determined by the deformation gradient matrix and ρ_0 is the reference density.

The energy equation

$$\dot{E} = V s_{ij} \dot{\epsilon}_{ij} - (p+q)\dot{V} \tag{2.6}$$

is integrated in time and is used for equation of state evaluations and a global energy balance. Deviatoric stresses and pressures, s_{ij} and p, in the energy are denoted as

$$s_{ij} = \sigma_{ij} + (p+q)\delta_{ij}, p = -\frac{1}{3}\sigma_{ij}\delta_{ij} \tag{2.7}$$

with q as the bulk viscosity and $\dot{\epsilon}_{ij}$ as the strain rate tensor.

The solver uses a standard finite element formulation to solve the equations above at discrete intervals determined by the mesh density.

2.5 Fluid Structure Interaction

For the fluid structure interaction LS-DYNA the immersed boundary method. Not much is disclosed of how this is implemented [11], but what is known is that the FEM solver employs a Lagrangian frame for the structural part whereas for the fluid part the CESE solver uses an Eularian frame. This Lagrangian structure is what dictates the locations and velocities for the boundary locations at the interface between fluid and structure meshes and is updated at each time step. The CESE solver communicates back the fluid pressures to the structural interface to be used as exterior forces in the structural solver.

3 Method

Every simulation in this report was run using the CESE module for compressible flow in the commercial software LS-DYNA by LSTC. The input to the software is in the form of a "Solution Deck" that consists of "Input cards", and each card describes an aspect of either the fluid domain or the structural analysis. The complete workflow can be viewed in Figure 3.1.

3.1 Software used in the project

3.1.1 MATLAB

MATLAB is a very powerful software able to interpret code and execute very high-level commands and can easily perform complicated calculations. In this project the program was primarily a tool for plotting data when analyzing the numerical and analytical solutions derived in the project. When solving the wedge problem described in section 4.2 a regressive algorithm implemented in the function `fzero()` in the optimization toolbox [12] had to be used while solving the Prandtl-Meyer function as it is not analytically solveable. This tool was also useful for converting the load curves for mass flow that was designed for the previous simulations of gas generators.

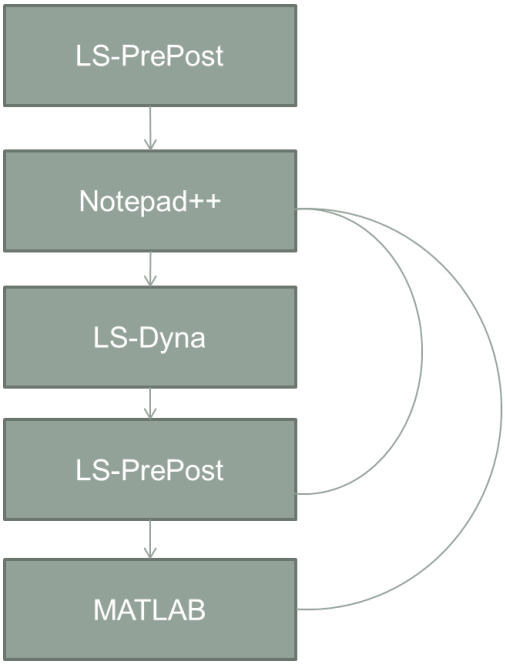

Figure 3.1: *The general workflow applied in the project*

3.1.2 LS-PrePost

Henceforth know as LSPP, this program is a Pre/Post processor developed by LSTC to be used exclusively to set up and analyze decks for LS-DYNA. In the beginning of the project LSPP version 4.0 was used, but this had no support for the cards used in the CESE-solver and crashed when trying to open a CESE project.

3.1.3 ANSA

ANSA is a meshing tool that was used. During the project it was discovered that LS-DYNA performs best when using a structured mesh made up of hexagonal volume cells. This was not apparent in the beginning of the project as the CESE solver comes with a function for automatic meshing that builds a volume part from tetragonal volume elements even though the CESE theory manual [9] states that the CESE solver in LS-DYNA can handle tetragonal elements equally well as hexagonal.

3.1.4 LS-DYNA

LS-DYNA is a multiphysics solver developed by Livermore Software Technology Corporation and is extensively used in a variety of applications[13]. This program have the ability to link different physics solvers together, e.g. performing Fluid Structure Interaction (FSI) analysis, making it a very powerful design tool for engineers. The cards contain all the information needed for the solver to run a simulation. In the appendix you will find some of the cards that were used some cases. Information on the properties of each card is not covered in this thesis, but can be found in the LS-DYNA manual vol III [14]. LS-DYNA Version able to successfully run all of the cases: mpp d Dev revision 96595 (beta version).

3.2 Hardware used in the project

The simulations were mainly run at Chalmers Centre for Computational Science and Engineering on the PC-cluster named Beda. It has a total of 268 nodes, 2144 cores, and about 7 TB of RAM. Nehalem CPUs (Xeon E5520, 2.27GHz) with 4 cores per CPU socket, and 8 cores per computational node. The run time comparisons in this project were made when using 1 core.

3.3 Simulations

In the coming chapters you will find a brief explanation of the different simulations used in this project to assess the performance of the CESE solver.

3.3.1 Sod's shock tube

The one dimensional shock tube problem (also known as Sod's shock tube problem [15]) is a widely used benchmark case within the field of compressible fluid mechanics. In this project, it has been used to validate the numerical simulation in LS-DYNA using an analytical approach in MATLAB.

Sod's shock tube problem consist of a 1 meter long tube with a diaphragm in the middle of it (Figure 3.2). The diaphragm separates two regions at different states; one region with high pressure, and one region with low pressure. At time $t = 0$ the diaphragm is destroyed and the gas/gases are free to search equilibrium in the tube.

The process that occurs while equilibrium is setting in is well known and also analytically solvable, making this experiment a very easy one to test out the accuracy of a solver for compressible flow.

This test has been used before by LSTC to prove the validity of their CESE solver. The complete test is not available for review, and therefore a new and independent trial was decided upon. The analytical solution was evaluated in MATLAB and the numerical simulation was run using the CESE solver in LS-DYNA. After the simulation some measuring points were sampled to compare the two results in MATLAB.

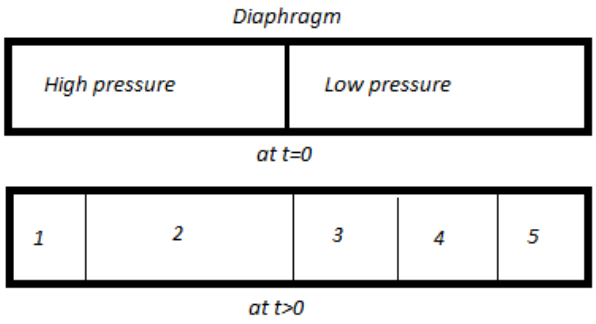

Figure 3.2: *Initial conditions and formed areas after diaphragm is released at t=0*

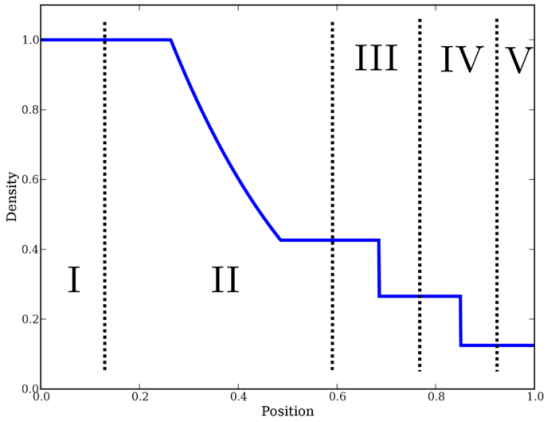

Figure 3.3: *Sod's shock tube problem, picture licensed under public domain and available at http://en.wikipedia.org*

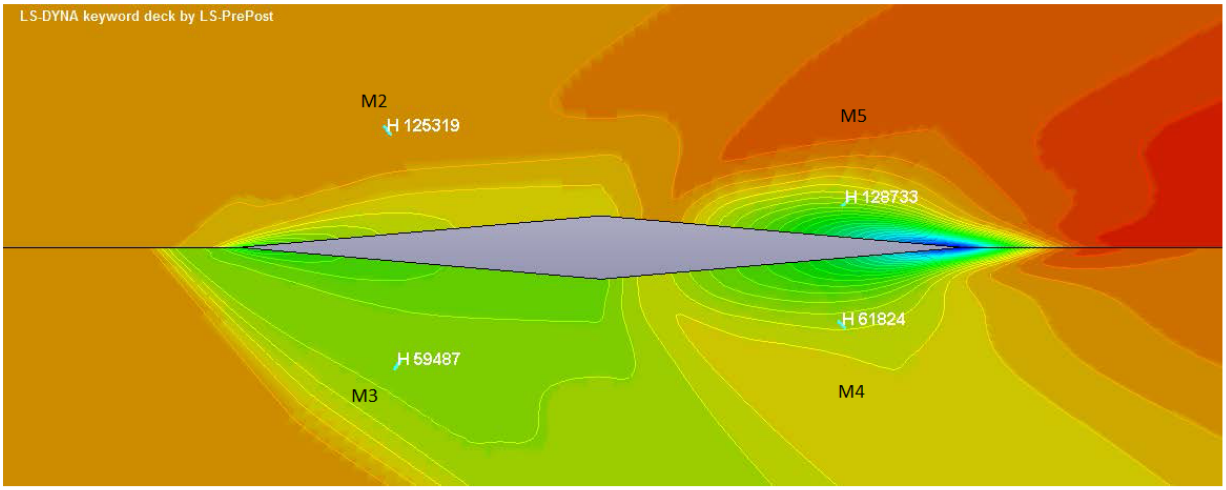

Figure 3.4: *Fluid velocity plot of flow around a wedge*

3.3.2 Wedge example

To further evaluate the proficiency of the code to simulate discontinuities in flow situations a wedge simulation was run. This case also has an analytical solution which will be used to validate the results from the numerical simulations in LS-DYNA using the CESE-scheme. The simulation was first meant to be run in 3D, but after initial runs proved that to be way too costly, a 2D approach was formulated instead. The mesh density used in this case was as high as possible to get the simulation to be able to run in a reasonable amount of time. To get the full simulation time of 16 seconds through the run had an estimated time of 1,533 hours (one core on BEDA), but as the program outputs data at quantified increments the simulation was stopped when a steady-state solution was found.

The results were then compared to an analytical solution made in MATLAB. This comparison can be viewed in Figure 5.1. Some explanation is needed to properly evaluate the results. The different Mach numbers are referring to specific areas of the flow which are sampled at a point in the numerical simulation and calculated in the analytical solution. M1 is referring to the free flow, M2 - M5 are referencing quadrants around the wedge. Since the flow has an incidence angle of 2^o a uniform behavior of the flow around the wedge was not expecter. The picture is there to show where the data samples had been taken.

3.3.3 Tank test

The primary tool for developing a method of analysis using the CESE solver was a tank test that had been used previously to validate models of gas generator. A tank test is nothing more than a body of a set volume where the effects of different boundary conditions can be studied. The nodes in the walls were locked in place and are thereby not influenced by the fluid. This was the primary cause of introducing this test, but it showed itself to be highly useful for trying out different approaches to FSI.

In previous efforts to simulate an expanded A-pillar a coupled Euler-Lagrange method has been used to simulate the flow from the gas generator. To model the gas flow from the gas generators a set of vectors were defined and a mass flow was coupled to these vectors. More

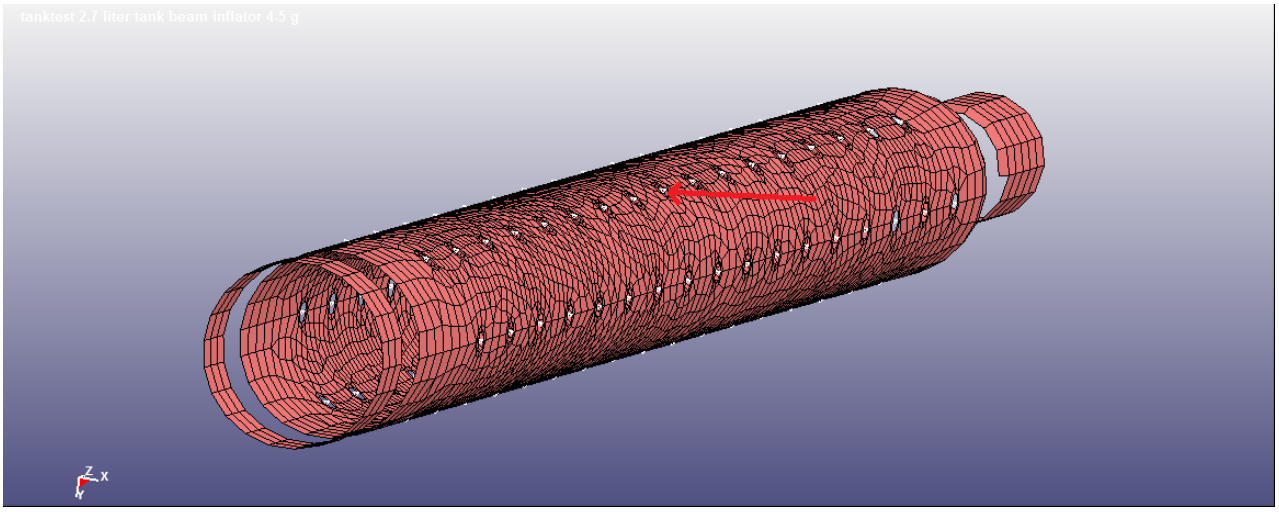

Figure 3.5: *Previous model of a gas generator.*

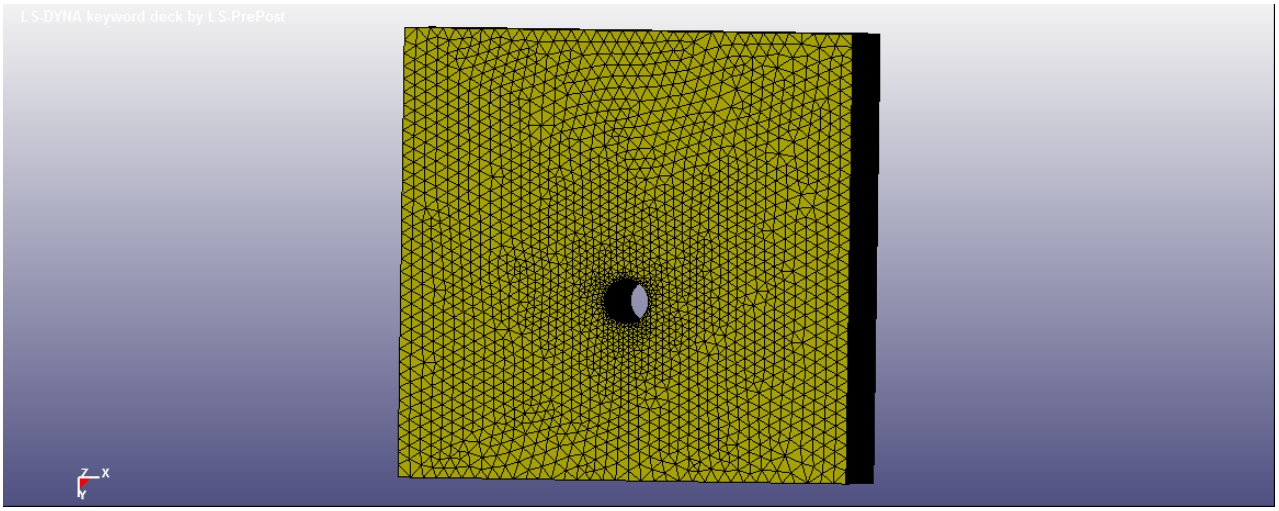

Figure 3.6: *Model of tank prepared for use with automatic meshing.*

specifically these vectors were placed in the nodes in the middle of the outlet holes as can be viewed in Figure 3.5 (red arrow pointing at one). With the CESE solver this approach is not valid anymore. Therefore several attempts to replicate the behavior of the gas generator have been made. In every simulation in this section a tank of constant volume was used to compare different techniques.

Automatic meshing

There is an example of the automatic mesher involving fluid structure interaction available from LS-DYNA. In this example a sheet of embedded shell elements being affected by the flow is simulated. The coupling between the CESE and the structural solver proved in the current project to be quite unstable when trying to simulate a more complex object (the wedge example following in a later section) than a sheet of shell elements.

If using the automatic meshing tool (which is not recommended by the developers of the CESE solver) included in LS-DYNA it is possible to fill the outlet holes in the gas generator model as shown in Figure 3.5 with shell elements, define six parts correlating to the six

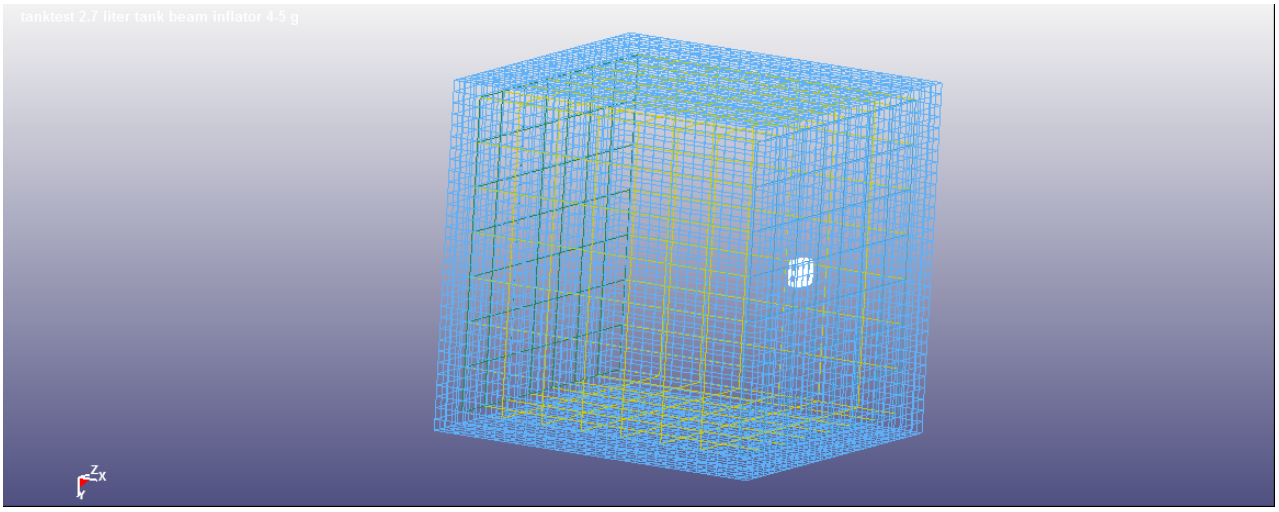

Figure 3.7: *Tank of shell elements inside fluid domain and inlet inside tank.*

different circle sectors which should have identical boundary conditions, divide the flow in to u vs v components, and couple these to the corresponding parts. This approach is very straight-forward and of course the first one to be tried.

The surface mesh of the tank test when automatic meshing was applied, seen in Figure 3.6, needed to be modified so as to use the gas generator housing as an external boundary of the fluid domain. Otherwise the boundary conditions could not be applied.

The mesh density of the automatically generated mesh can be affected by changing the size of the surface shell elements. This can be useful to control different mesh parameters, like controlling the y^+-values[1] for the simulation to keep somewhat consistent simulations. Such mesh analysis in post processing is not available in LS-DYNA, which is also why no mesh dependence study was made. When contacting the developers of the software with the problem of how to ascertain that the flow is resolved correctly they had no recommendation. Furthermore, this approach suffered the same symptom as all other efforts of using the automatic meshing tool; it was slow. Run times were quickly reaching hundreds of hours even for this simple example.

Hexagonal mesh inside the domain

The second approach was done using a fixed mesh consisting of hexagonal volume elements in the fluid domain. This approach proved to be much easier to run and run times were significantly decreased. The main issue with using this approach is that it can only be applied on very basic and preferably rectangular domains and a very complex shape, like the A-pillar, is not possible to mesh.

Hexagonal mesh and immersed boundary with inlet inside tank

The third approach was done using a predefined domain of hexagonal volume elements which is large enough to have the tank completely immersed. This approach has been used in LS-DYNA before, unlike the previous two, and was immensely easier to set up and get to run. Several attempts were made with different kinds of boundary conditions, but to no avail. Later on

[1] a ratio that couples fluid velocity to cell size

it was divulged from the developers that the CESE solver does not support inlet boundary conditions on an internal boundary of the computational domain. This was a set back since this is what the project was aiming to simulate.

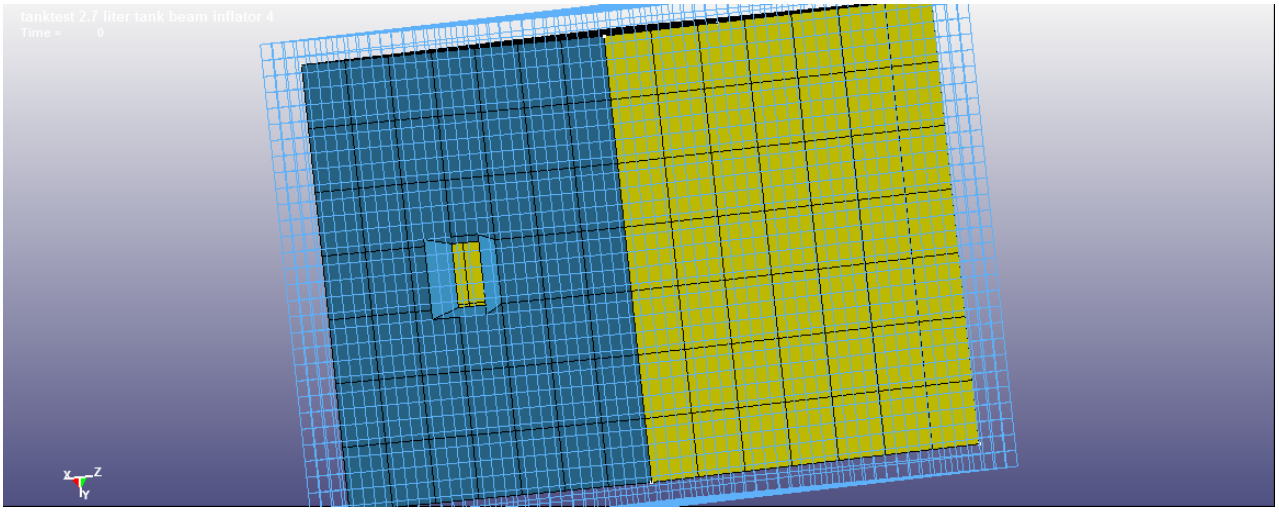

Figure 3.8: *Tank with a funnel inside hexagonal mesh.*

Hexagonal mesh and immersed boundary with inlet outside tank

The fourth and final approach to developing a method of analysis was done by building a funnel of shell elements from the outside of the fluid domain to the inside of the tank, see Figure 3.8 for image. With this approach, the flow could be simulated. As in previous situations the only way of defining the inlet boundary conditions was to use a segment set at the outside of the fluid domain.

Tetragonal VS hexagonal

Both tests were identically defined when it comes to computational domain, boundary conditions, fluid properties, and everything else that is controllable in LS-DYNA. The element size was sampled as a characteristic size at the inlets where the flow velocity will be the greatest and, therefore, the element size will have to be the smallest. The total number of elements is in a comparative range as you can fit two tetragonal elements in one hexagonal and that is also the order of magnitude that we can observe in the difference in size between the two meshes. It should also be noted that the ”automatic” part in automatic meshing means that there is no control at all when it comes to how the mesh will be created other than making the shell elements of the outside domain larger or smaller. The automatic mesher will make the mesh gradually finer when it approaches a shell mesh of finer density than on the other side.

3.3.4 A-pillar

The final model of the A-pillar, Figure 3.9 was built using the approach that proved the most reliable in producing viable results during the tank test, i.e. with immersed boundary and boundary conditions on the outside of the computational domain. In the presented figure some of the fluid mesh has been cut away to show the funnel that needed to be constructed to lead the gas in to the A-pillar.

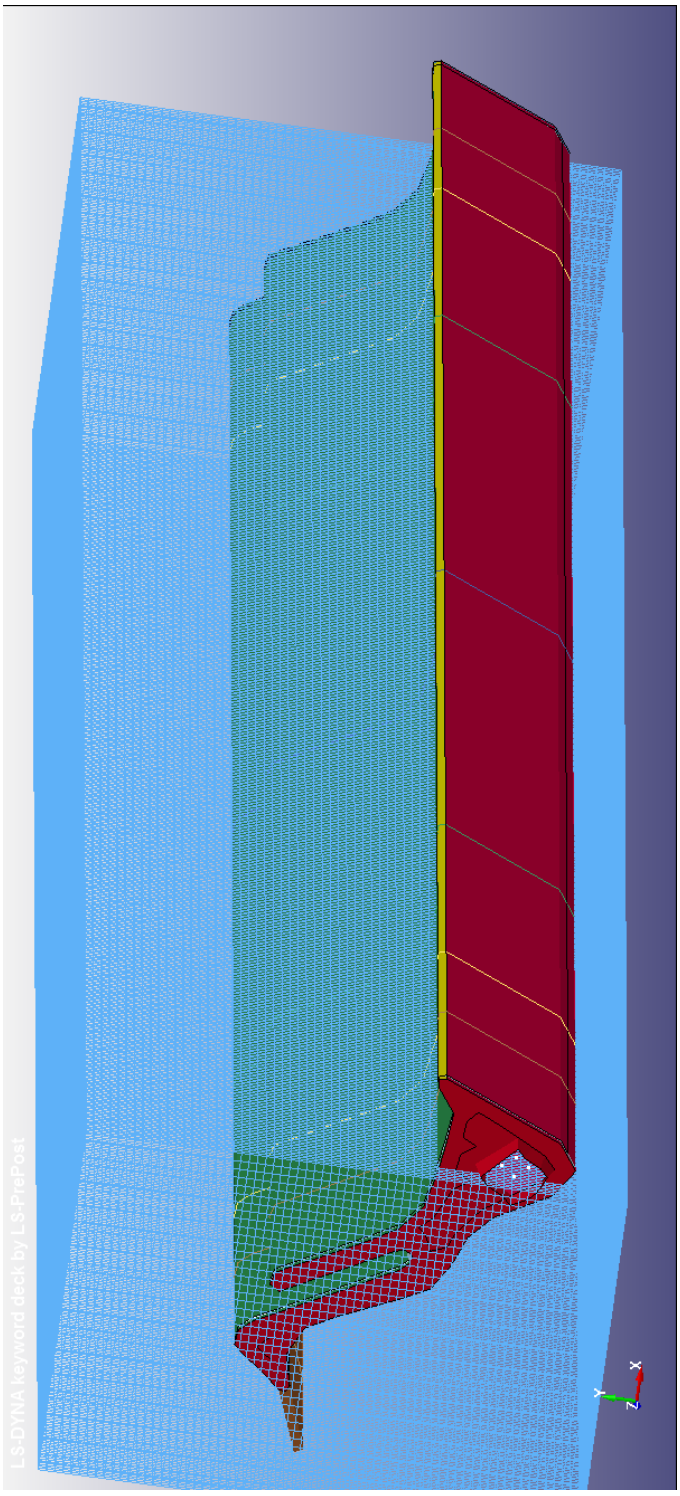

Figure 3.9: *Model of the A-pillar with a funnel inlet*

BC: load curves

Based on the input cards of previous simulations using the corpuscular particle model and the model of the gas generator that was used therein, a set of boundary conditions could be established by scaling the mass flow $[\frac{kg}{ms}]$ to quantities that the CESE solver can use as boundary conditions.

BC: extracted pressure

The pressure at the surface of the gas generator in the corpuscular particle method was sampled and extracted to form load curves pertaining to the pressure at the inlet of the CESE model of the A-pillar.

BC: constant pressure

A constant pressure boundary condition at the inlet of the CESE model of the A-pillar.

4 Analytical Calculations

4.1 Sod's shock tube

Starting with the initial conditions which are illustrated in Figure 3.2 we will define these as, ρ=density [kg/m^3], P=pressure [Pa], u=velocity [m/s], index L and R refer to the left and right domain respectively:

$$\begin{pmatrix} \rho_L \\ P_L \\ u_L \end{pmatrix} = \begin{pmatrix} 1.0 \\ 1.0 \\ 0.0 \end{pmatrix}, \begin{pmatrix} \rho_R \\ P_R \\ u_R \end{pmatrix} = \begin{pmatrix} 0.125 \\ 0.1 \\ 0.0 \end{pmatrix} \tag{4.1}$$

To solve this problem we start by defining the speed of sound for the regions furthest from each other when $t > 0$

$$a_1 = \sqrt{\gamma \frac{P_L}{\rho_L}}\ ,\ a_5 = \sqrt{\gamma \frac{P_R}{\rho_R}} \tag{4.2}$$

with $\gamma = 1.4$ for the case of air at standard conditions (100 kPa, 273.15 K) [16] after which we can form the coefficients

$$\Gamma = \frac{\gamma - 1}{\gamma + 1}\ ,\ \beta = \frac{\gamma - 1}{2\gamma} \tag{4.3}$$

Using these coefficients we can relate the density in region 5 to the one in region 4 using

$$\rho_4 = \rho_5 \frac{P_4 + \Gamma P_5}{P_5 + \Gamma P_4} \tag{4.4}$$

which is the Rankine-Huginot shock jump condition with Γ as explained above. This requires that we must know the pressure in region 4 to calculate the density in region 4. Thankfully the contact discontinuity (a density discontinuity with constant pressure) dictates that the

pressure in region 4 will be the same as the pressure in region 3, $P_4 = P_3$, which can be calculated iteratively using the following equations and with P_3' as the guessed quantity and β from Equation 4.3[15]:

$$u_4 = (P_3' - P_5)\sqrt{\frac{1-\Gamma}{\rho_R(P_3' + \Gamma P_5)}} \tag{4.5}$$

$$u_2 = (P_1^{\beta} - P_3'^{\beta})\sqrt{\frac{(1-\Gamma^2)P_1^{\frac{1}{\gamma}}}{\Gamma^2 \rho_L}} \tag{4.6}$$

$$\tag{4.7}$$

$$u_2 - u_4 = 0 \tag{4.8}$$

A function is formed using equations 4.5 and 4.6 that can be solved iteratively for the parameter P_3. This gives us the information needed to evaluate the expressions

$$u_3 = u_5 + \frac{(P_3 - P_5)}{\sqrt{\frac{\rho_5}{2}((\gamma+1)P_3 + (\gamma-1)P_5)}} \tag{4.9}$$

and

$$u_4 = u_3 \tag{4.10}$$

Finally using the adiabatic gas law we get

$$\rho_3 = \rho_1 \big(\frac{P_3}{P_1}\big)^{\frac{1}{\gamma}} \tag{4.11}$$

4.2 Flow around a wedge

This example, which can be viewed in Figure 4.1, was used to study the effects of formed shockwaves caused by obstructing objects in the flow. This case also has an analytical solution which will be used to validate the results from the numerical simulations in LS-DYNA using the CESE-scheme.

Starting of with defining the initial conditions for the case:

$$\begin{aligned} M1 &= 1.0 \text{ Mach (340 m/s)} \\ T1 &= 300 \text{ K} \\ p1 &= 101325 \text{ Pa} \\ \theta_2 &= 2^{\text{o}} \\ \theta_3 &= 8^{\text{o}} \\ \gamma &= 1.4 \\ L &= 0.2 \text{ M} \\ \alpha_w &= 3^{\text{o}} \end{aligned}$$

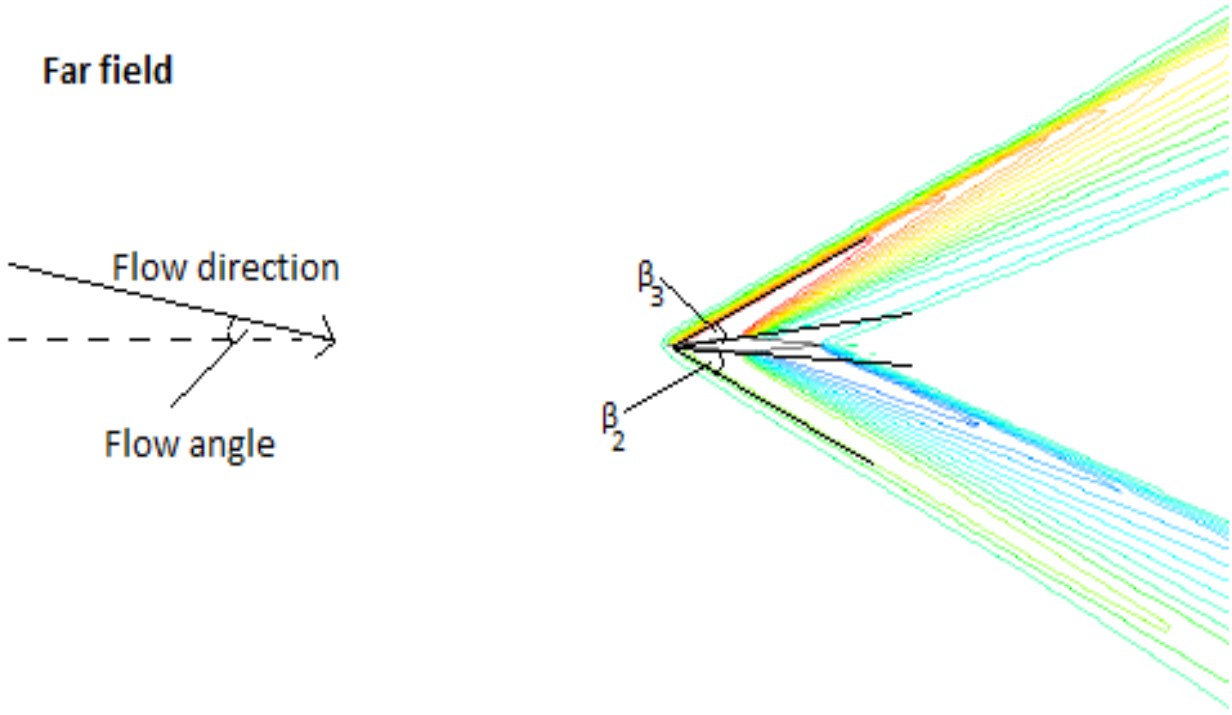

Figure 4.1: *Pressure contours from previous study of this case. For illustrative purposes only. Figure taken from the course material for TME085, Compressible Flow, at Chalmers University of Technology*

with $M1$ as the free flow Mach number, $T1$ as the far field temperature, $p1$ as the far field pressure, θ_2 as the lower flow deflection angle (flow angle - half tip angle), θ_3 as the upper flow deflection angle (flow angle + half tip angle), γ as before, L is the chord length (how long the object is in the direction of the flow) of the wedge and α_w is the incidence angle of the flow which is shown as the flow angle in Figure 4.1.

To solve the flow parameters analytically for this example we must first calculate the oblique shock angles formed by the obstructing object in the flow. This is done using the θ-β-Mach relationship [17] which is a non-linear relationship that can either be approximated using tables or solved using an iterative algorithm. The author chose the second route.

This relationship is described as (when solved for β):

$$\beta(M,\theta,\gamma,n) = atan(\frac{b+9ac}{2(1-3ab)} - \frac{d(27a^2c+9ab-2)}{6a(1-3ab)}tan(\frac{n\pi}{3}+\frac{1}{3}atan(\frac{1}{d})))\frac{180}{\pi} \tag{4.12}$$

where n in this case is equal to zero since we want the first reflection wave. At even higher air flow velocities, more and much fainter shock waves are formed at angles described by other β-values. All other quantities in the above equation are described as:

$$\begin{aligned}
\theta &= \theta\frac{\pi}{180} \\
\mu &= asin(1/M) \\
c &= tan(\mu)^2 \\
a &= (\frac{(\gamma-1)}{2}+(\gamma+1)\frac{c}{2})tan(\theta) \\
b &= (\frac{(\gamma+1)}{2}+(\gamma+3)\frac{c}{2})tan(\theta) \\
d &= \sqrt{4\frac{(1-3ab)^3}{((27a^2c+9ab-2)^2)}-1}
\end{aligned}$$

This gives us the oblique shock wave angles (β_2 and β_3 as shown in Figure 4.1)

$$\beta_2 = \beta(M_1,\theta_2,\gamma,0)\ ,\ \beta_3 = \beta(M_1,\theta_3,\gamma,0); \tag{4.13}$$

The normal component of the air flow speed is preserved across shockwaves [18] and therefore we use this to take the next step in our analysis.

$$M_{n,low,before} = M_1 sin(\beta_3)\ ,\ M_{n,high,before} = M_1 sin(\beta_2); \tag{4.14}$$

From this we can calculate the normal Mach number after the shock

$$\begin{aligned}
M_{n,low,after} &= \sqrt{\frac{M^2_{n,low,before}+\frac{2}{(\gamma-1))}}{\frac{2\gamma}{\gamma-1}M^2_{n,low,before}-1}} \\
M_{n,high,after} &= \sqrt{\frac{M^2_{n,high,before}+\frac{2}{(\gamma-1))}}{\frac{2\gamma}{\gamma-1}M^2_{n,high,before}-1}}
\end{aligned}$$

and from this we can deduce the pressures in both zones after the oblique shock waves

$$p_2 = p_1(1 + \frac{2\gamma}{\gamma+1}(M^2_{n,low,before} - 1))$$
$$p_3 = p_1(1 + \frac{2\gamma}{\gamma+1}(M^2_{n,high,before} - 1))$$

and also the Mach numbers

$$M_{low,after} = \frac{M_{n,low,after}}{sin(\beta_2 - \theta_2)} \ , \ M_{high,after} = \frac{M_{n,high,after}}{sin(\beta_3 - \theta_3)} \tag{4.15}$$

To take the next step in our analysis we must utilize the Prandtl-Meyer function, ν Equation 4.16, which describes the behavior of the flow when it exhibits a so called expansion fan; a phenomenon occurring when the fluid domain expands leading to a gradually diminishing pressure and rising air speed. It looks very much like a multicolored fan when simulating in CFD software.

$$\nu(M,\gamma) = \sqrt{\frac{\gamma+1}{\gamma-1}}atan(\sqrt{\frac{\gamma-1}{\gamma+1}(M^2-1)}) - atan(\sqrt{M^2-1}) \tag{4.16}$$

With the two states

$$\nu_2 = \nu(M_{low,after}, \gamma) \ , \ \nu_3 = \nu(M_{high,after}, \gamma) \tag{4.17}$$

the Prandtl-Meyer function is utilized as:

Define the turn angle of the flow as $\varphi = 10^o$ (the blunt angle on the wedge) and use the relation $\varphi = \nu(M_{low,afterExpansion}) - \nu(M_{low,after})$ and correspondingly $\varphi = \nu(M_{high,afterExpansion}) - \nu(M_{high,after})$.

This is not analytically solvable and using a numerical solving method, e.g. the function `fzero` in MATLAB a corresponding case can be set up. After which the pressures in the regions after the expansion fans are easily calculated as:

$$\begin{aligned} p_4 &= p_2(\frac{1 + 0.5(\gamma-1)M^2_{low,after}}{1 + 0.5(\gamma-1)M^2_{low,afterExpansion}})^{\frac{\gamma}{\gamma-1}} \\ p_5 &= p_3(\frac{1 + 0.5(\gamma-1)M^2_{high,after}}{1 + 0.5(\gamma-1)M^2_{high,afterExpansion}})^{\frac{\gamma}{\gamma-1}} \end{aligned}$$

5 Numerical Results

Initially Sod's Shock Tube was used as a benchmark case, after that a more complex, but also analytically solvable, case was analyzed, the wedge example. After that followed a run-time comparison between automatic and manual meshing. Then the modelled gas generator had to be converted to work with the CESE method. A previous model of the gas generator was already available, however it was not compatible. The resulting load curves from the convertion to CESE has been based on the existing gas generator model for the particle method

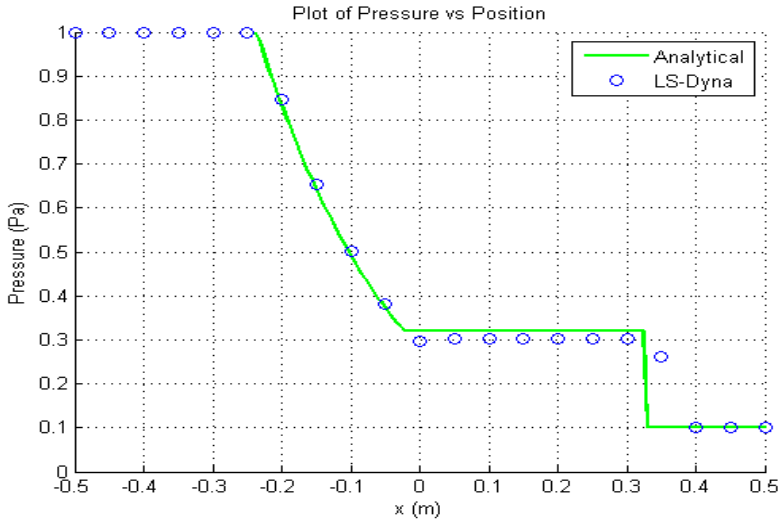

Figure 5.1: *Comparison between the analytical solution and the simulation using the CESE solver in LS-DYNA*

solver. Finally a simulation of an expanding A-pillar could be made. Below the results from all simulations can be found.

The results are focused on the pressure quantity since the fluid structure interaction is communicated only by using pressure. There may be many valid points to be made regarding other quantities such as flow velocity, vorticity etc., but these will not be covered in this report.

5.1 Sod's shock tube

The results of the comparison can be seen in Figure 5.1. In this case the numerical dissipation was kept low ($\alpha_{LS-DYNA} = 2, \beta_{LS-DYNA} = 1, \epsilon_{LS-DYNA} = 0.5$), but it still needs to be present to get the solution to converge.

Version of LS-DYNA able to succesfully run the case: R7.1.1.

5.2 Wedge example

Table 5.1: Comparison between the analytical solution and the simulation using the CESE solver in LS-DYNA

	M1	M2	M3	M4	M5
Calc [m/s]	340	384	463	510	579
Sim [m/s]	330	373	286	311	403
Diff	2.9%	2.8%	38.3%	39.0%	30.3%

In Table 5.1 M2 and M3 are the leftmost quadrants around the wedge with M2 being the one at most direct angle of attack towards the flow.

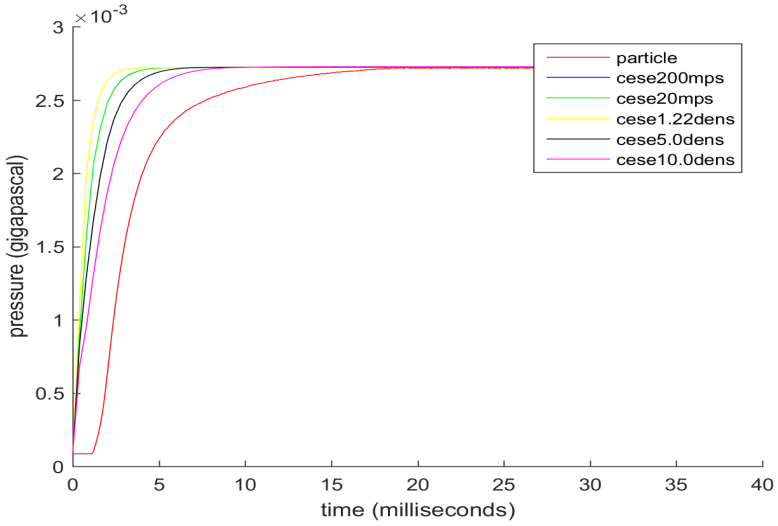

Figure 5.2: *Study made to see what parameters affected the pressure at the far wall.*

5.3 Tetragonal VS hexagonal

Table 5.2 shows a run time comparison between hexagonal meshing (which is made by hand) and automatic tetragonal meshing.

	Element size (mm)	Total number of elements	Estimated run time
Automatic	0.24	5 356 365	31 941 hrs 43 mins
Hexagonal	0.26	3 012 746	1 648 hrs 31 mins

Table 5.2: Run time comparison between two possible meshing types.

5.4 Conversion of gas formulation from previous model

Below the numerical results from the conversion from legacy mass flow to a load curve formulation consistent with the CESE solver can be found.

5.4.1 Weighting using constant density at the inlet

To accurately measure the converted flow from the previous case of a mass flow defined with directional vectors the resulting pressure were sampled at the wall furthest from the inlet. A study was made on the parameters that the user was able to vary, the results of which can be seen in Figure 5.2. The inlet velocity did not affect the pressure at the far wall. In addition, it could be concluded that the rise time to final pressure was greatly affected by the density at the inlet.

The first inlet density chosen was the density of Nitrogen as it was defined in the Euler-Lagrange model of the gas generator since it is the primary gas expelled from a gas generator. For this density value, the rise time of the pressure was much too fast. This is expected since the gas in the generator is compressed before the membrane bursts and the gas is free to be transported out into the domain.

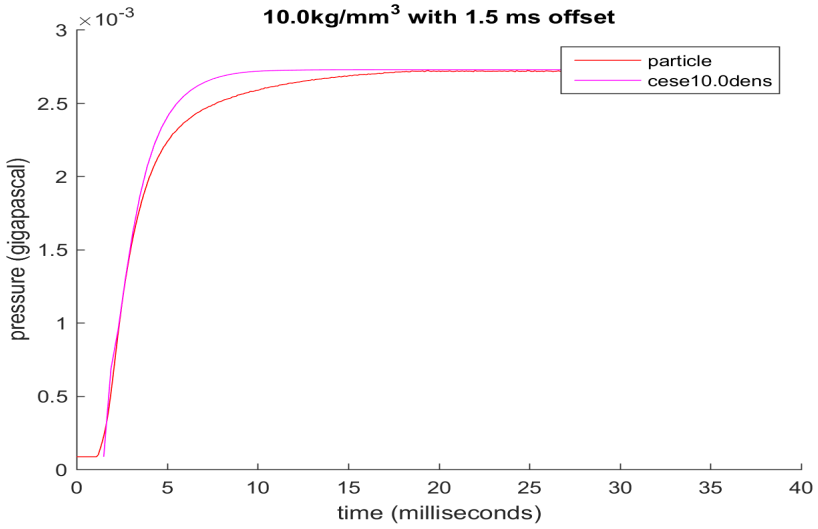

Figure 5.3: *Result from variation study.*

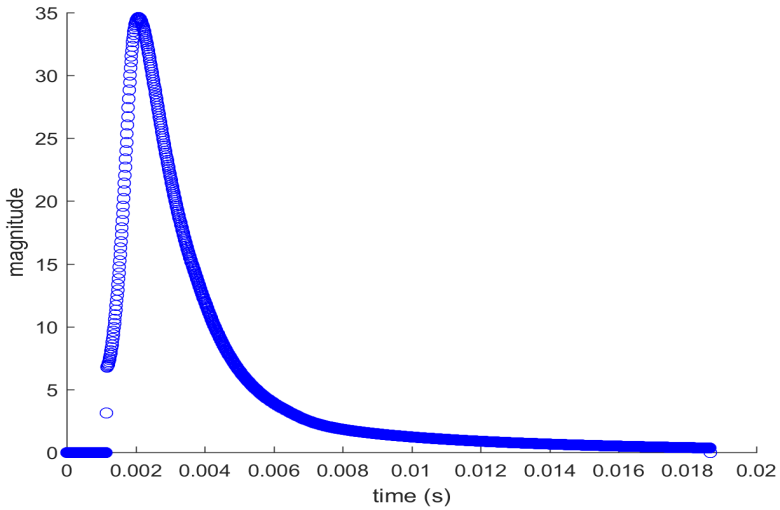

Figure 5.4: *Load curve from particle simulation.*

By varying the magnitude of the density at the inlet with a constant pressure boundary condition a value of 10.0 kg/mm^3 was derived. Both curves can be seen overlaid in Figure 5.3.

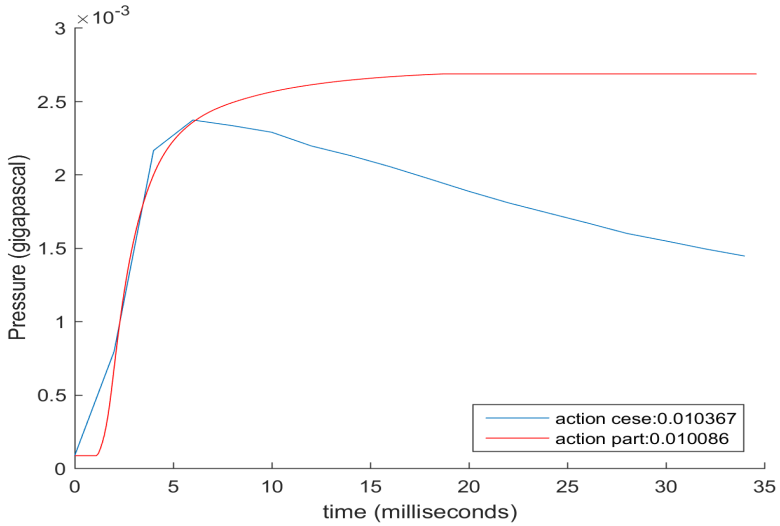

Figure 5.5: *Comparison between far wall pressure curve effects from the CESE load curve and particle method.*

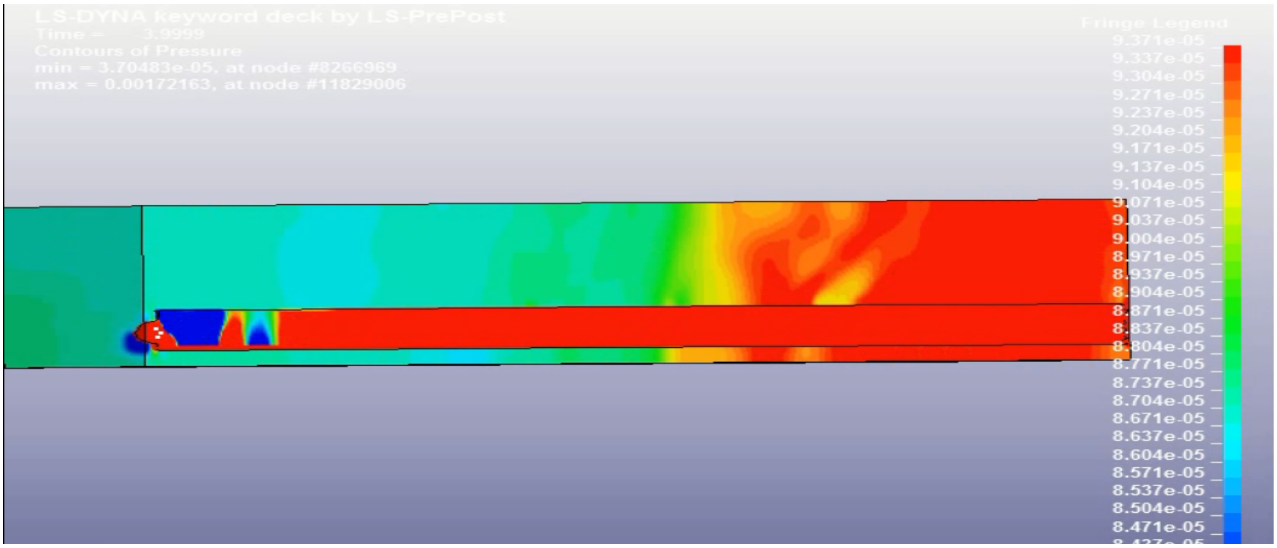

Figure 5.6: *Severe leakage problems apparent in the model shown as pressure increase outside of the A-pillar*

5.5 Expanding A-pillar

These are the results from the different set ups used to analyze the expanding A-pillar.

5.5.1 BC: load curves

The load curve in Figure 5.4 was applied to inlet velocity, density and pressure and was scaled to have the same magnitude as in the particle experiment [2]. Figure 5.6 display a pressure plot of a cross section of the computational domain, inlet to the left. The red colored ”pipe” with black borders is the inside of the A-pillar whereas everything outside of this is the exterior domain.

5.5.2 BC: extracted pressure

By extracting a pressure curve from the particle experiment a more accurate representation of the gas generator can be achieved. In this trial the pressure at the inlet was controlled by the load curve that was extracted from the particle test while the density, velocity and temperature where set as constants, also based on the Euler-Lagrange experiment. Three trials were made using this boundary condition; one with the fluid domain completely enclosing the A-pillar, one where the fluid domain comes up short of the far side of the A-pillar, effectively cutting of the top end and removing the possibility of leakage through the shell elements, and one where also the inlet part where cut off and the fluid domain was shorter than the length of the A-pillar.

Whole domain

The results of the trial with only boundary conditions changed were basically identical with the previous trial with load curve controlled boundary conditions. The leakage can be viewed in Figure 5.7 as a dramatic rise in fluid velocity outside of the confines of the A-pillar.

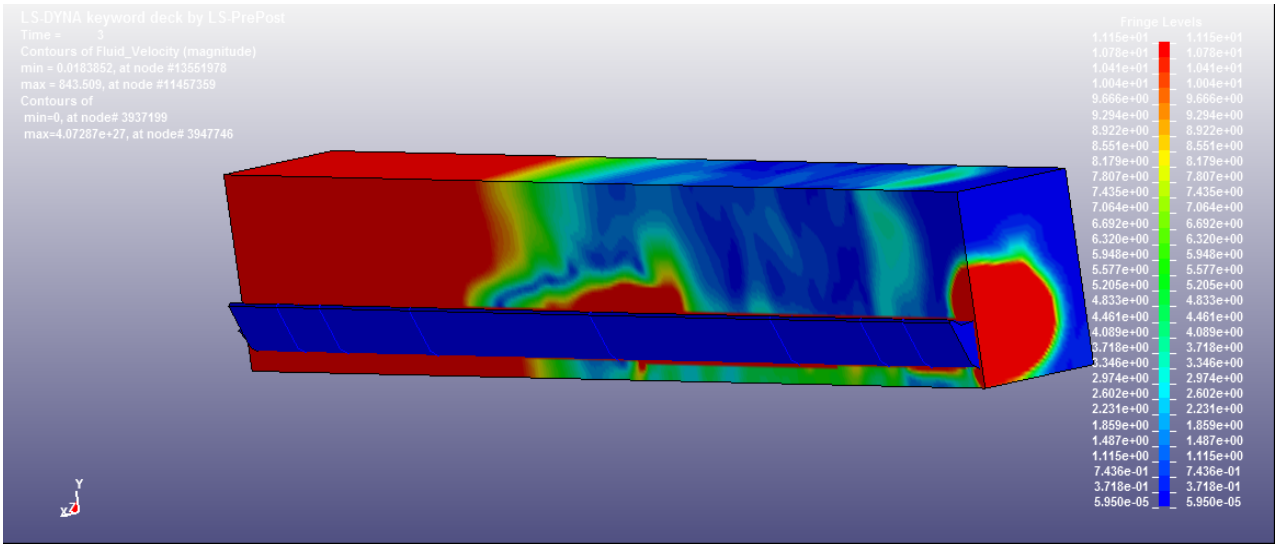

Figure 5.7: *Fluid velocity plot from particle test, whole domain*

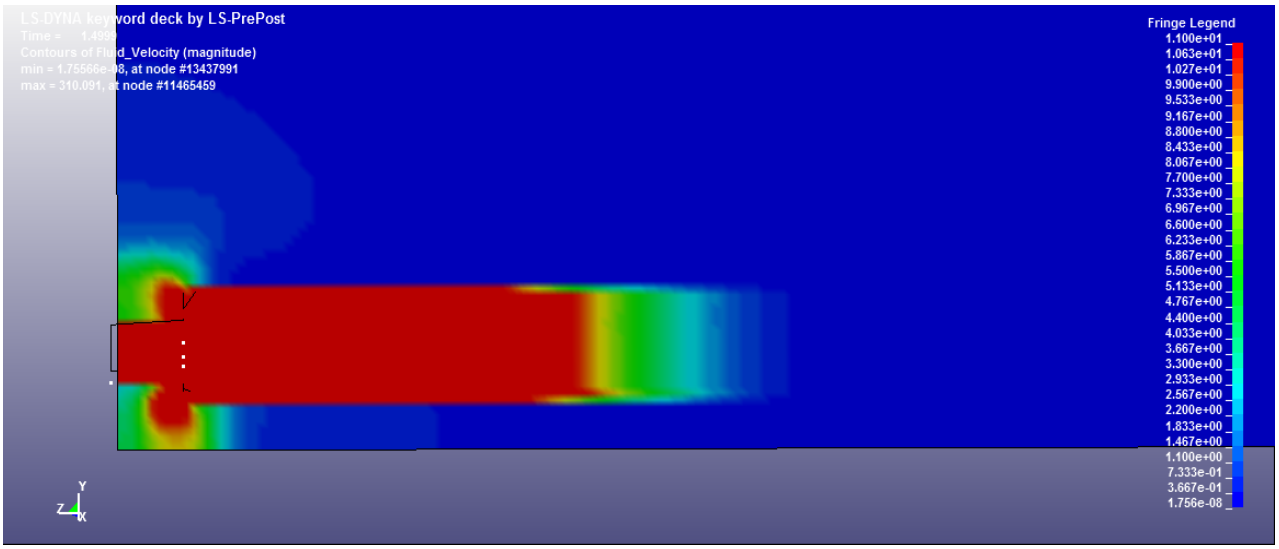

Figure 5.8: *Fluid velocity plot with the far side of the A-pillar outside of fluid domain*

One end cut off

To alleviate the symptom of leakage at the far end a trial was made were the shock wave was allowed to be reflected on a surface with reflecting boundary condition instead of relying on a fluid structure interaction coupling to supply a surface for reflection. This trial was most successful at removing the effects of leakage at the far end, but still no expansion could be produced. Upon inspection a leakage was found at the inlet (see Figure 5.8) where the gas was allowed to escape the confines of the A-pillar.

Both ends cut off

The third and final run made using the extracted pressure curves from the particle experiment were set up with the fluid domain shorter than the length of the A-pillar, effectively negating the effects of leakage at both the reflecting side and at the inlet.

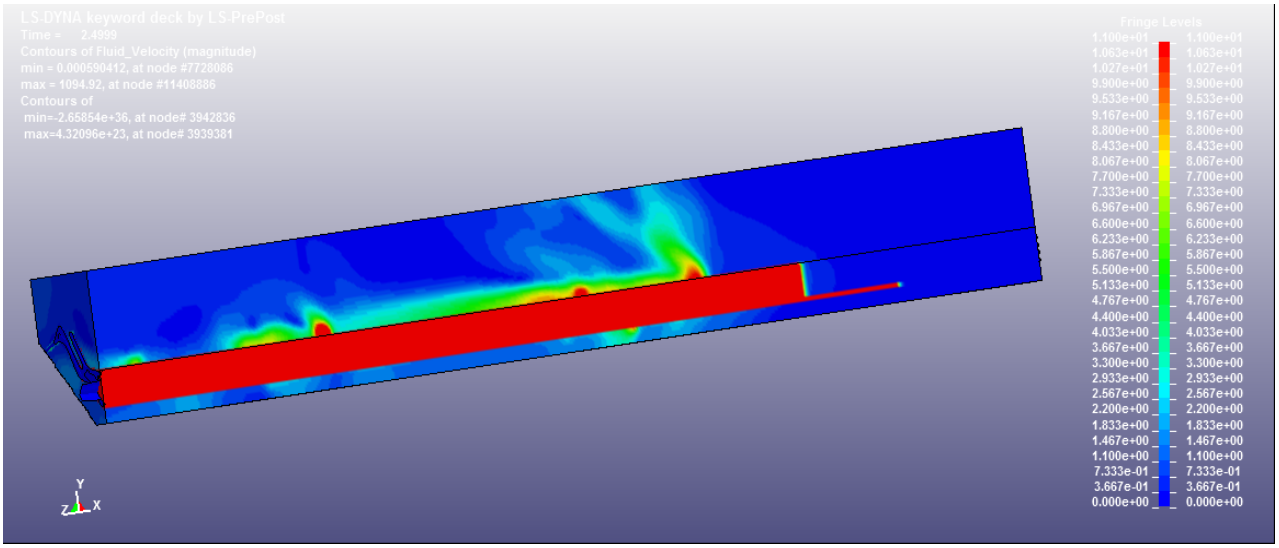

Figure 5.9: *Leakage apparent by plotting fluid velocity with both inlet and reflecting side outside of the bounds of the fluid domain*

In Figure 5.9 the resulting fluid velocities of the run can be seen at a time before the shock wave hitting the reflecting side.

5.5.3 BC: constant pressure

As a proof of concept a run with boundary condition with a constant pressure was made. The magnitude of pressure was raised until a stable simulation was no longer possible. The simulation crashed after 2.8 ms elapsed time (about 96 hours runtime on 16 cpus on Beda), but expansion was achieved before this. A comparison between the measured pressure inside the A-pillar with constant BC and a measurement from the particle BC can be seen in Figure 5.11.

A side-by-side comparison between the resulting expansion in the case of BC:s using load curves from the particle test and the case with constant BC:s can be seen in Figure 5.14.

6 Discussion

6.1 Sod's shock tube

The numerical dissipation in the experiment might have lead to the discrepancy in results between the analytical solution and the simulation after the discontinuity. The dissipation could not be lowered lest the solution would diverge. What can be observed also is a very good concordance between the numerical solver and the analytical solution (see Figure 5.1) with a slight undershoot in the numerical simulation at the expansion. After the expansion there is some loss of coherence between the analytical solution and the simulation, also a possible side effect of the dissipation.

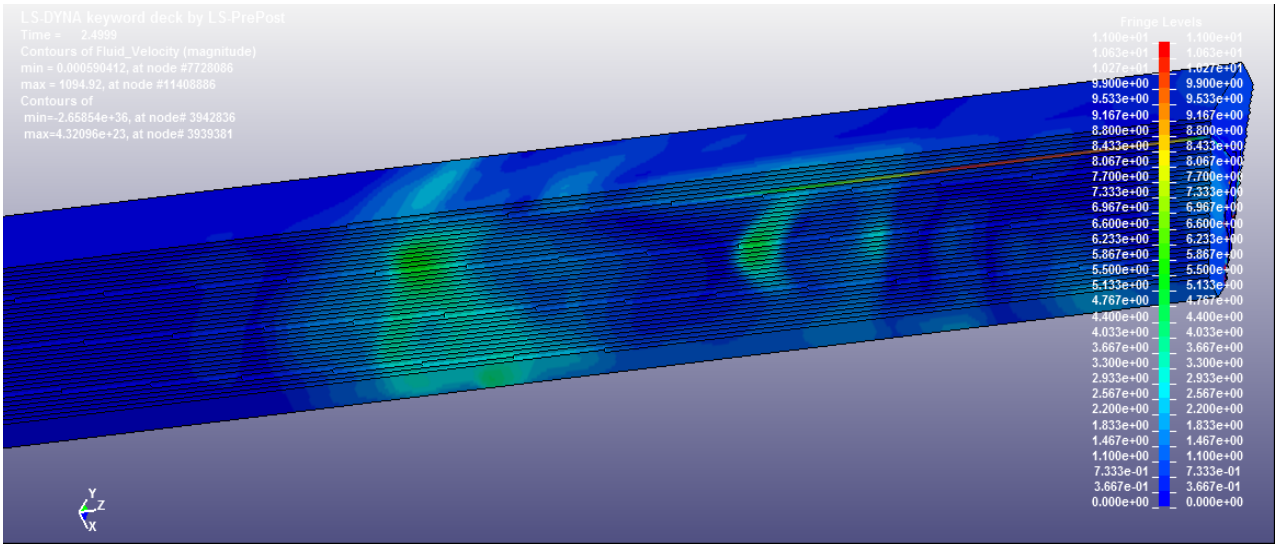

Figure 5.10: *Same run as in Figure 5.9, but showing leakage through fluid velocities in the domain on the other side of the A-pillar*

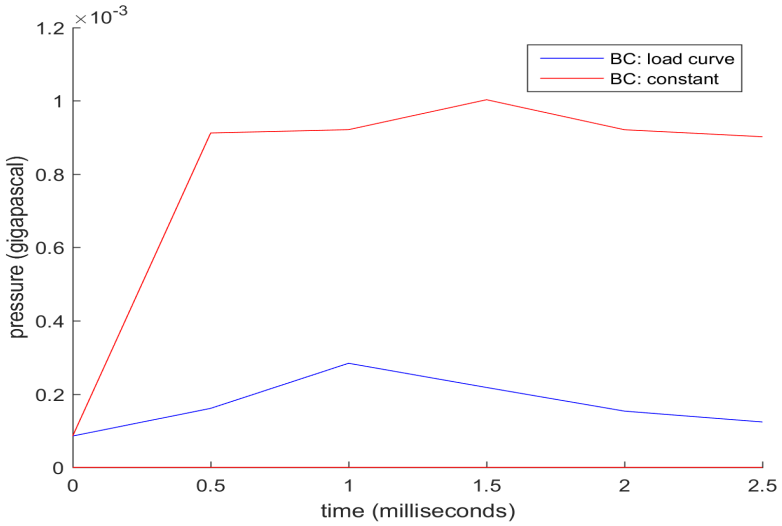

Figure 5.11: *Resulting pressure comparison close to the end nearest the inlet*

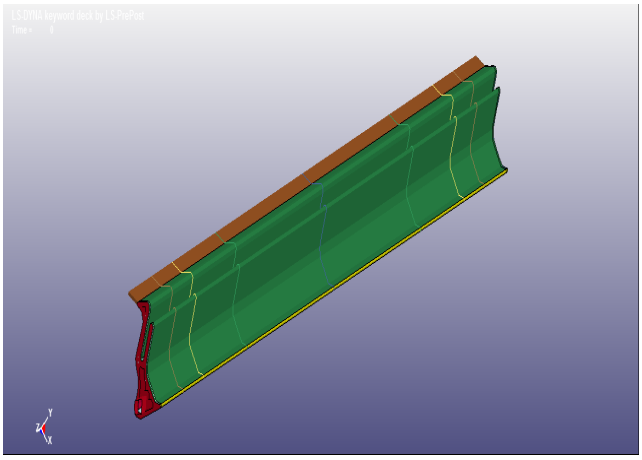

(a) *Expansion at t=0.0 ms*

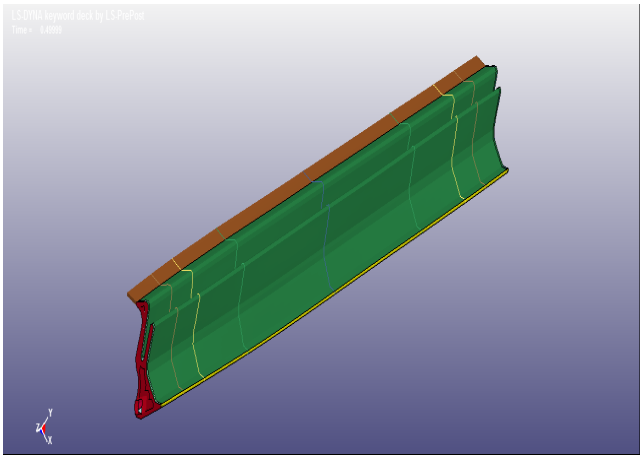

(b) *Expansion at t=0.5 ms*

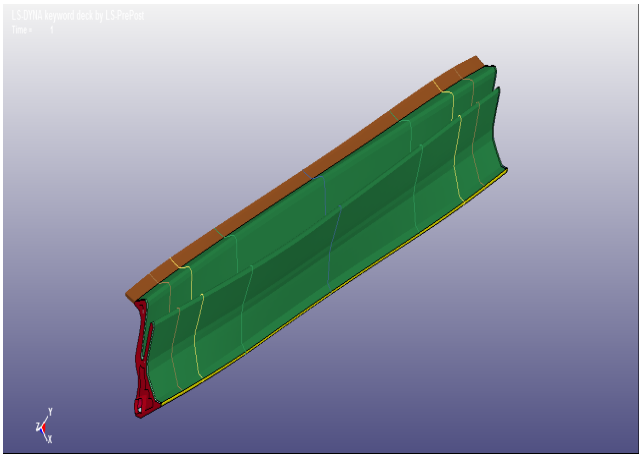

(c) *Expansion at t=1.0 ms*

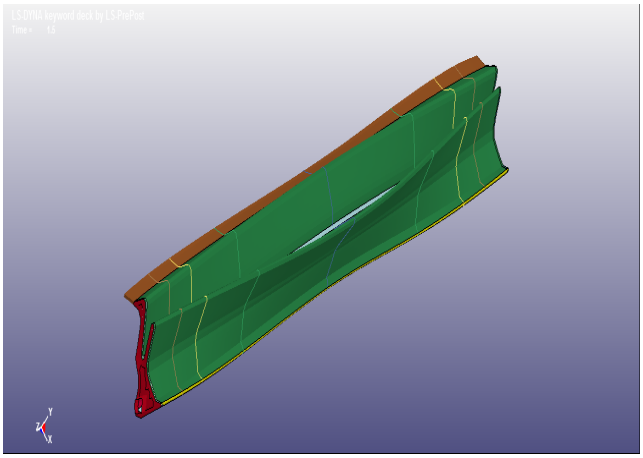

(d) *Expansion at t=1.5 ms*

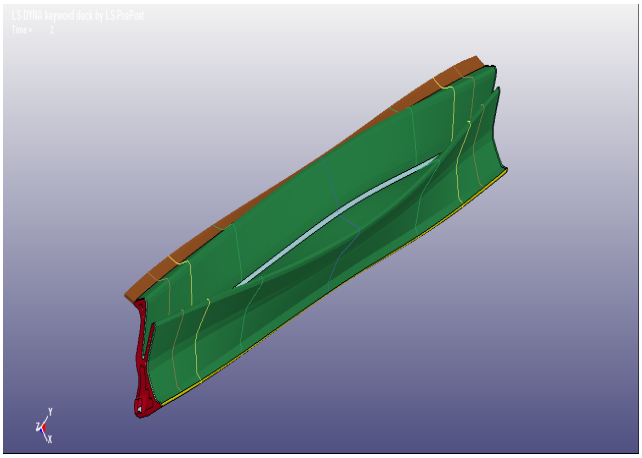

(e) *Expansion at t=2.0 ms*

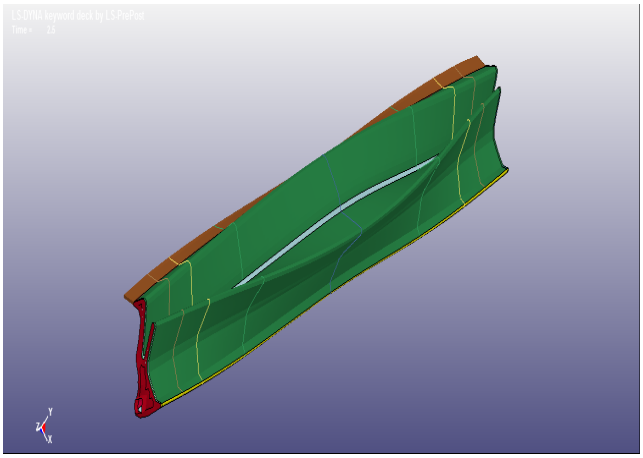

(f) *Expansion at t=2.5 ms*

Figure 5.12: *Expansion at constant pressure*

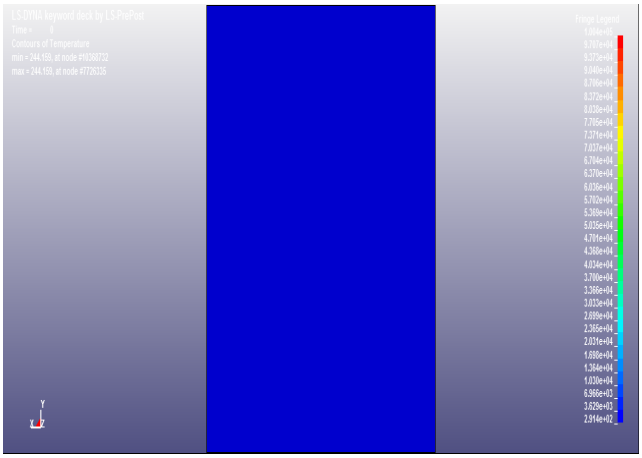

(a) *Temperature at t=0.0 ms, scale from 291 K to 100,000 K*

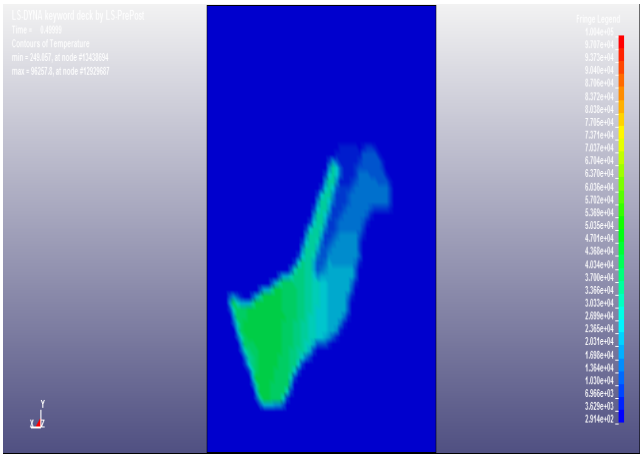

(b) *Temperature at t=0.5 ms, scale from 291 K to 100,000 K*

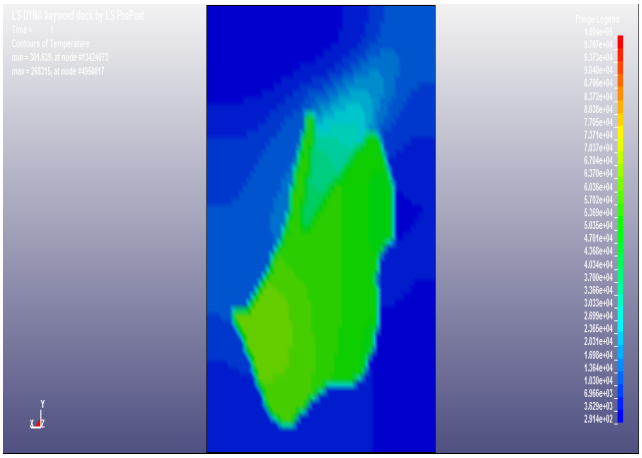

(c) *Temperature at t=1.0 ms, scale from 291 K to 100,000 K*

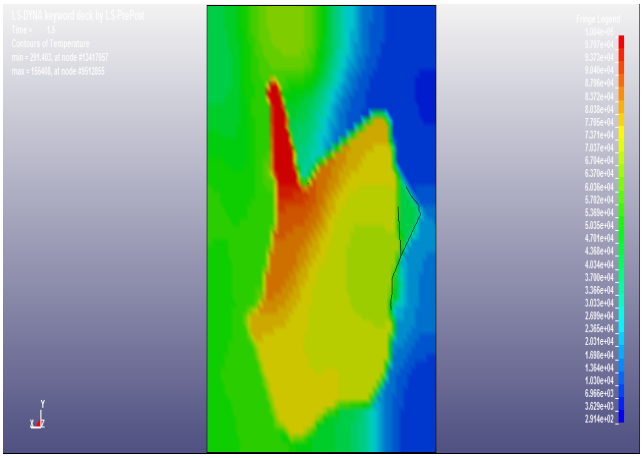

(d) *Temperature at t=1.5 ms, scale from 291 K to 100,000 K*

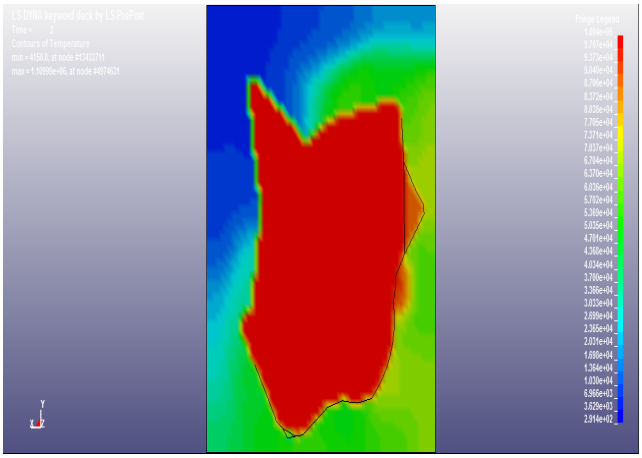

(e) *Temperature at t=2.0 ms, scale from 291 K to 100,000 K*

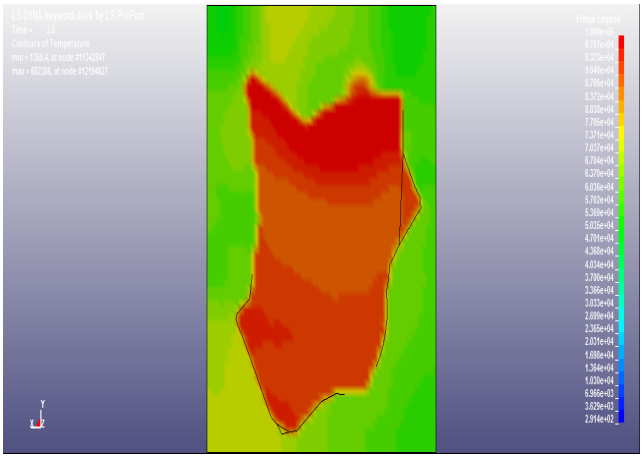

(f) *Temperature at t=2.5 ms, scale from 291 K to 100,000 K*

Figure 5.13: *Temperature plot at constant pressure*

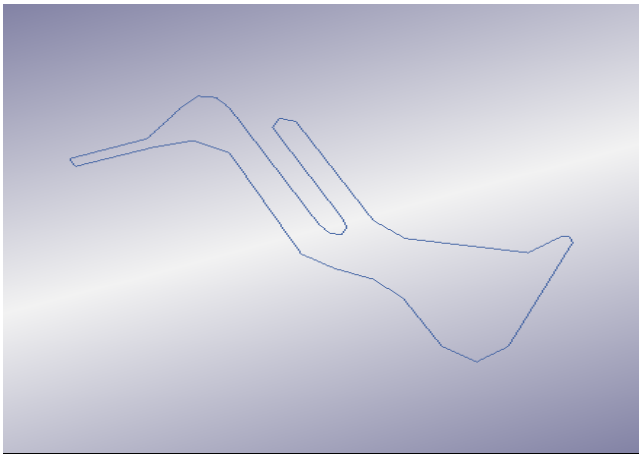

(a) *Particle BC at t=0.5 ms*

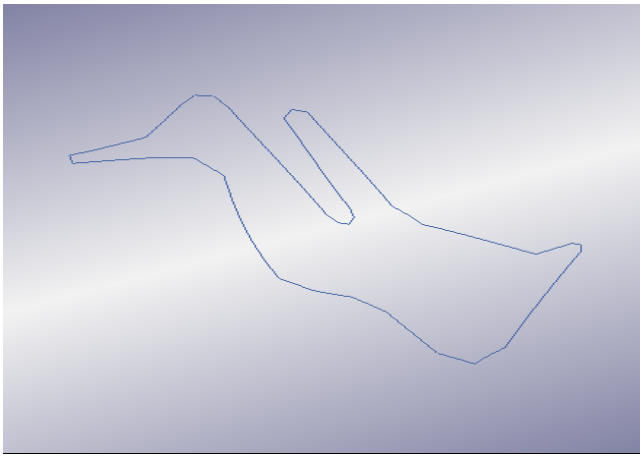

(b) *Constant BC at t=0.5 ms*

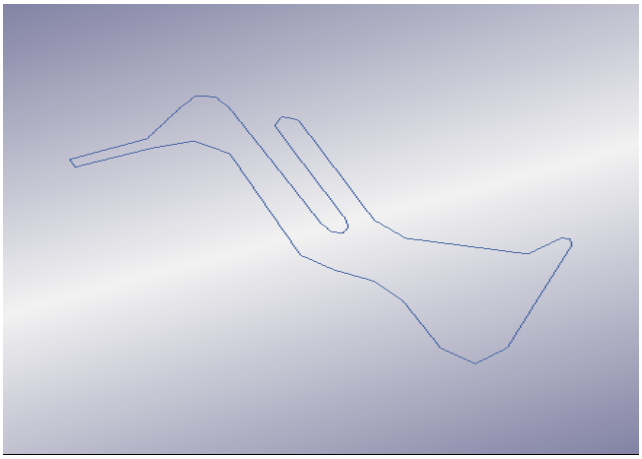

(c) *Particle BC at t=1.5 ms*

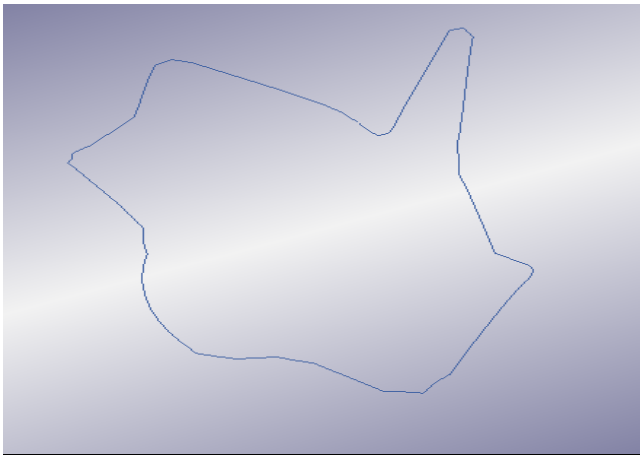

(d) *Constant BC at t=1.5 ms*

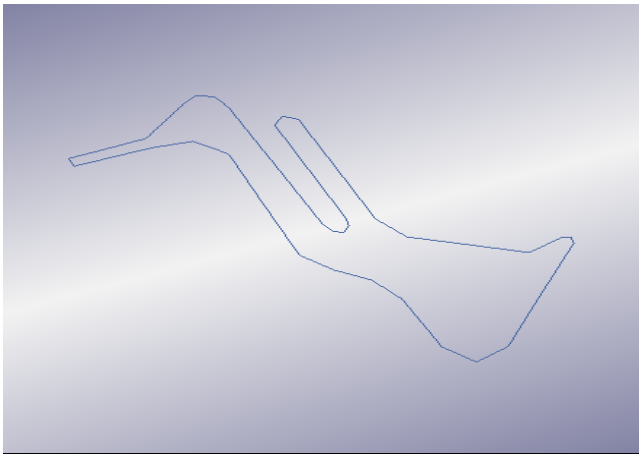

(e) *Particle BC at t=2.5 ms*

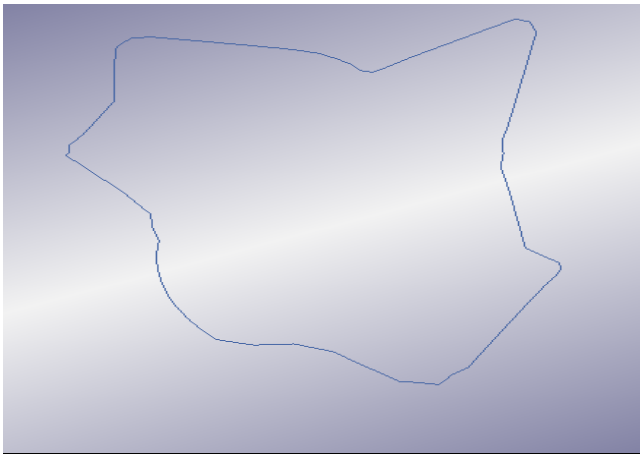

(f) *Constant BC at t=2.5 ms*

Figure 5.14: *Side-by-side comparison between resulting expansion of a cross section from particle BC and constant BC*

6.2 Wedge example

In this scenario a large discrepancy between analytical and numerical solutions is observed. Initially this might be seen as an indication of the solver not being able to handle strong oblique shocks, and it may well be true, but considering the high amount of numerical dissipation that was applied to this case ($\alpha_{LS-DYNA} = 2, \beta_{LS-DYNA} = 1, \epsilon_{LS-DYNA} = 0.5$) to keep it stable the results are not that surprising. Notice that these values are the same as in the previous example with Sod's shock tube, and in that case these amounts were considered low. This is because of the sharp discontinuities that needed to be resolved in the previous case whereas in this case the changes in flow quantities are more incremental and does not necessitate high amounts of numerical diffusion to get a converged solution.

Here we can find a very good concordance between numerical and analytical simulation, which bodes well for the A-pillar expansion since that is the kind of flow diversion that will be most affluent in that case.

6.3 Tetragonal VS hexagonal

As stated in the method chapter the information from LS-DYNA is that the CESE solver can handle both tetragonal and hexagonal elements. As the program comes with an easy to use automatic meshing possibility this was the obvious way to go at first, but this approach was soon to be changed. A run time comparison was made by using a time estimation that was output from LS-DYNA after a few time steps had been resolved. The results from the comparison can be seen in Table 5.2.

The comparison shows us that this simulation using the hexagonal meshing (which is made by hand) has an estimated runtime 20 times less than that of the case with the automatic tetragonal meshing. Therefore no more automatic meshing was used in this project.

Version of LS-DYNA able to successfully run the case: mpp d Dev revision 92881 (beta version).

6.4 Conversion of gas formulation from previous model

Starting with the exported load curve from the previous Euler-Lagrange simulation, Figure 5.4, the inlet flow was simulated with the load curve applied to both the inlet velocity and the pressure, keeping the density constant at 10 kg/mm^3. To validate this model the integrated pressure, $\hat{P} = \int_{t=0}^{t_1} P(t)dt$, on the far side of the domain was examined. Looking at the the previous experiments of expanding an A-pillar using the particle model, it was ascertained that full expansion had occurred after 4.3 ms. This time was set as t_1 for the action calculations. After this we can evaluate the expression as the area under the P(t) curve during the first 4.3 milliseconds in a P-t graph.

Looking at Figure 5.5 we see a 3 % difference between the resulting $\hat{P}$ on the far wall in the two different methods. A difference which partly stems from the resolution of the measuring method of the CESE curve. This result is good enough to carry on to the A-pillar simulation for the purpose of this report.

The significant different response of the curves post pressure wave can be explained by comparing how the different boundary conditions are implemented. In the particle case there

is a mass flow which can be interpreted as a source term in the PDE, causing the overall pressure to rise without any outer inlet, whereas in the CESE case an inlet could not be applied within the computational domain and therefore the gas can flow out of the inlet segment after expansion, causing this downward trend after expansion. Since the full expansion should already have occurred before this happens, it has been assumed that the post-peak response does not affect the simulation of the expanding A-pillar.

6.5 Expanding A-pillar

If the first run would have been successful the inside in Figure 5.6 would be red and little to no pressure rise would be registered in the outside domain (when the A-pillar expands some pressure rise is expected due to the movement of a boundary surface). What can be observed from the results of this run is an apparent leakage at the far side of the A-pillar leading to pressurized gas being able to escape into the outside domain, pressure on the inside of the A-pillar drops to sub plastic levels where the stresses are too small to cause plastic deformations and no expansion can occur.

In Figure 5.9 three red semicircles can be seen above the long red rectangular section. These semicircles mark the approximate location of three points of leakage. Effects like these could be found regardless of direction of cross section, another can be viewed in Figure 5.10, implying that there is severe leakage apparent in the model. No expansion can occur as long as the model is leaking and the ”trick” that has been used so far can not be applied further.

The resulting pressure in figure 5.11 is not that great, even though a very high pressure has been chosen at the inlet.

The expansion proved that a complex structure can be affected using an immersed boundary method and the CESE solver. It can be seen in Figure 5.12 and temperature in the fluid elements of a cross section in the middle of the A-pillar can be seen in Figure 5.13. Worth noticing in Figure 5.13 is the approximate temperature of 97,000 K stemming from the high pressure at the inlet. The disparity between this measurement and the relatively modest pressure increase inside the A-pillar viewed in Figure 5.11 is also very indicative of leakage problems.

7 Summary and Conclusions

During the process of simulating the expanding A-pillar the following observations were made:

The immersed boundary method must be used It is not possible to only mesh the fluid domain inside of the A-pillar and let the outside boundary be influenced by the fluid inside.

Mesh quality can not be analyzed with the tools provided by LSTC It is not possible to measure local values for y^+, CFL, etc. in the postprocessor to find where a finer mesh could be needed. Neither is the automatic meshing advanced enough to re-mesh between iterations if the fluid properties require it.

The CESE-method performs well when simulating shock waves, less so when simulating expansion fans During the wedge examples both phenomena could be observed in the same simulation and referring to the differences viewed in Table 5.1 a large error can be seen after the expansion fans.

The CESE-solver is much faster when solving for a structured mesh of hexagonal volume elements than using an unstructured mesh of tetragonal elements In Table 5.2 the expected time to completion for both automatic and hexagonal meshing is seen and there is a factor 10 of difference to be gained by doing the meshing by hand.

It is not possible model the gas flow from the gas generator using only the CESE solver, but it is possible to simulate the behavior using load curves The CESE-solver does not support the same input cards as the particle solver where the rate of creation of a gas is defined and the flow is affected accordingly. The way around this was to sample the definable quantities in the particle simulation and then applying the load curves on the CESE simulation.

Boundary conditions must be applied on the outside of the computational domain, not on an internal boundary There is no support in the code for application of boundary conditions on a segment inside of the outmost segment according to the developers. There is no information on this in the manual.

Only faces of the hexagonal cells in the fluid domain can be used for application of boundary conditions The hexagonal cell itself can not have properties of the fluid prescribed.

There is leakage apparent in the simulation of the expanding A-pillar The conclusion of the simulations of the expanding A-pillar is that severe leakage is apparent, the cause of which could not be found by neither the author nor the developers at LSTC.

The immersed boundary method made setting up fluid structure interaction quite simple. Sadly, no comparison of the A-pillar could be done with other models or physical tests since the cause of the leakage apparent in the model could not be found during the project.

8 Further Work

The work on defining the model of a gas generator to CESE compatible input cards is not yet completed. What has been done in this report is an extremely coarse adaptation to make the model fit within the boundaries of this project. Here are a couple of suggestions to further develop an apt model of the gas generator.

First of all it is proposed that the CESE solver should be coupled with the CHEMISTRY solver. The CHEMISTRY solver seems to have been developed side-by-side with the CESE solver since the release on more detailed documentation on both has come in the same drafts. The coupling between the two can be done with the
`*CESE_INITIAL_CHEMISTRY` card and by defining a gas composition with the
`*CHEMISTRY_COMPOSITION` card. Together with this, the initial condition can be coupled to

a list of elements, very much so as was the first approach in this report to simulate the gas generator. However, it does not say in the manual if these elements should be shell, volume, or any other kind of elements.

The leakage problem for the A-pillar has been an issue in previous models as well (although not reported on officially). The CESE method is supposed to be leakage proof [8] and it may very well be at the mathematical level. Whether the leakage in the simulation of the expanding A-pillar has its origin in the solver, the implementation in LS-DYNA, the model itself or any other reason is not known and the study of which falls outside the limitations of this thesis.

The ultimate goal to simulate an A-pillar of carbon fiber construction is not a large step to take. The structural solver in LS-Dyna is already prepared with material cards, and they should be compatible with the CESE-solver as well since the chosen material doesn't affect how the flow simulation manages the deformation. To successfully develop an expandable carbon fiber A-pillar the temperature plots found in Figure 5.13 can be very helpful to see if any cooling action is performed on the gas inside the expanding structure as it expands. Although, to accurately portray the temperature changes inside the domain a mesh density of at least twice [19] the one used in the project would be recommended.

References

[1] *Tacoma Narrows Bridge*. URL: https://en.wikipedia.org/wiki/Tacoma_Narrows_Bridge_\%281940\%29.

[2] Pipkorn Bengt Lundström Jesper EM. *SAFETY AND VISION IMPROVEMENTS BY EXPANDABLE A-PILLARS*. Autoliv, 11-0105.

[3] Acheson DJ. *Elementary fluid dynamics*. English. Oxford: Clarendon, 1990. ISBN: 019859660X; 9780198596608; 9780198596790; 0198596790. URL: www.summon.com.

[4] Davidson L. *Fluid mechanics, turbulent flow and turbulence modeling*. Division of Fluid Dynamics, Department of Applied Mechanics, Chalmers University of Technology, 2015.

[5] Majda A, Flow CF. Systems of conservation laws in several space variables. *Appl. Math. Sciences* **53** (1984).

[6] Nipun Kwatra Jón T. Grétarsson RF. *Practical Animation of Compressible Flow for Shock Waves and Related Phenomena*. Eurographics/ ACM SIGGRAPH Symposium on Computer Animation, 2010.

[7] *Space-Time Conservation Element Solution Element Method*. online. Accessed: 2015-05-25. URL: http://www.grc.nasa.gov/WWW/microbus/.

[8] Zeng-Chan Zhang Ia. *LS-DYNA® R7: Recent developments, application areas and validation results of the compressible fluid solver (CESE) specialized in high speed flows*. http://www.dynalook.com/9th-european-ls-dyna-conference/ls-dyna-r-r7-recent-developments-application-areas-and-validation-results-of-the-compressible-fluid-solver-cese-specialized-in-high-speed-flows. Accessed: 2015-05-25.

[9] *The CE/SE Compressible Fluid Solver*. online by LIVERMORE SOFTWARE TECHNOLOGY CORPORATION. URL: http://www.lstc.com/applications/cese_cfd/documentation.

[10] *LS-DYNA Theory Manual*. online by LIVERMORE SOFTWARE TECHNOLOGY CORPORATION. URL: http://www.lstc.com/applications/cese_cfd/documentation.

[11] *Fluid/Structure Coupling (FSI)*. online by LIVERMORE SOFTWARE TECHNOLOGY CORPORATION. URL: http://www.lstc.com/applications/cese_cfd/features/fsi.

[12] *Optimization toolbox for MATLAB*. online by Mathworks. URL: http://www.mathworks.com/help/pdf_doc/optim/optim_tb.pdf.

[13] *LSTC website*. http://www.lstc.com. Accessed: 2014-12-08.

[14] *LS-DYNA® KEYWORD USER'S MANUAL*. Version R7.0. LIVERMORE SOFTWARE TECHNOLOGY CORPORATION. 2013.

[15] Sod G. Survey of several finite difference methods for systems of nonlinear hyperbolic conservation laws (1978).

[16] *The Engineering Toolbox*. URL: http://www.engineeringtoolbox.com/stp-standard-ntp-normal-air-d_772.html.

[17] Rudd Lael Voneggers LMJ. Comparison of Shock Calculation Methods. *Journal of Aircraft* (1998). DOI: 10.2514/2.2349.

[18] Anderson JDJ. *Modern compressible flow : with historical perspective*. New York, Paris, 1982. URL: http://opac.inria.fr/record=b1079107.

[19] *Personal correspondence with the developers of the CESE solver*. Not published. Accessed: 2015-03-18.

[20] Chang SC. The Method of Space-time Conservation Element and Solution Element, a New Approach for Solving the Navier-Stokes and Euler Equations. *J. Comput. Phys.* **119**.2 (July 1995), 295–324. ISSN: 0021-9991. DOI: 10.1006/jcph.1995.1137. URL: http://dx.doi.org/10.1006/jcph.1995.1137.

[21] Çaldichoury ZCZI. Biotechnology at low Reynolds numbers. *Biophysical Journal* **71**.6 (Dec. 1996), 3430–3441. ISSN: 00063495. DOI: 10.1016/S0006-3495(96)79538-3. URL: http://linkinghub.elsevier.com/retrieve/pii/S0006349596795383.

[22] Svenning E. "Development of a nonlinear Finite Element beam model for dynamic contact problems applied to paper forming". MA thesis. Sweden: Chalmers University of Technology, 2011.

[23] Landau LD, Lifshitz EM. Fluid mechanics. 2nd Edition. English. *Oxford* (1987). URL: www.summon.com.

[24] Benoit Desjardins EG. *Low Mach number limit of viscous compressible flows in the whole space*. DOI: 10.1098/rspa.1999.0403. The Royal Society, 1999.

Appendices

A Settings

A.1 Sod's shock tube

In Tables A.1 - A.4 the cards for simulation of Sod's shock tube can be found.

Table A.1: Control cards for Sod's shock tube

*KEYWORD				
*TITLE				
Sod_1D_shock_tube				
*CESE_CONTROL_SOLVER				
iframe	iflow	igeom		
0	1	2		
*CESE_CONTROL_TIMESTEP				
iddt	cfl	dtint		
2	0.9	0.0001		
*CESE_CONTROL_LIMITER				
idlmt	alfa	beta	epsr	
0	2.0	1.0	0.5	
*CONTROL_TERMINATION				
endtim	endcyc	dtmin	endeng	endmas
1				

Table A.2: Initial conditions for Sod's shock tube

*CESE_INITIAL						
uic	vic	wic	rhoic	pic	tic	
0.0	0.0	0.0	0.125	0.1		
*CESE_INITIAL_SET						
setID	Duic	vic	wic	rhoic	pic	tic
111	0.0	0.0	0.0	1.0	1.0	
*CESE_PART						
pid	mid	eosid				
1	3					
*CESE_EOS_IDEAL_GAS						
eosid	cv	cp				
3	717.5	1004.5				

A.2 Super sonic flow around wedge

In Tables A.5 - A.9 the cards for simulation of the wedge example can be found.

Table A.3: Boundary conditions for Sod's shock tube

*CESE_BOUNDARY_NON_REFLECTIVE_SET
ssid
1
2
*CESE_BOUNDARY_REFLECTIVE_SET
3
4

Table A.4: Output settings for Sod's shock tube

*DATABASE_BINARY_D3PLOT			
dt/cycl	lcdt	beam	npltc
1.0e-1	0		
*INCLUDE			
mesh_ex1.k			
*END			

A.3 Tank test

In Tables A.10 - A.14 there are abbreviated cards to help with understanding what needs to be changed in the settings to evaluate the different setups. To save space only the important cards are included.

Table A.5: Control cards for wedge example

*KEYWORD				
*TITLE				
shock_boundary_layer_interaction				
*CESE_CONTROL_SOLVER				
iframe	iflow	igeom		
0	0	2		
*CESE_CONTROL_TIMESTEP				
iddt	cfl	dtint		
2	0.50	0.0001		
*CESE_CONTROL_LIMITER				
idlmt	alfa	beta	epsr	
0	4.0	2.0	0.0	
*CONTROL_TERMINATION				
endtim	endcyc	dtmin	endeng	endmas
2.0				

Table A.6: Initial conditions for wedge example

*CESE_INITIAL						
uic	vic	wic	rhoic	pic	tic	hic
333.48	47.64	0.0	1.225	1.01325e5		
*CESE_PART						
pid	mid	eosid				
1	7	5				
*CESE_MAT_GAS						
mid	c1	c2	prnd			
7	6.566e-6	0.9436	0.70			
*CESE_EOS_IDEAL_GAS						
eosid	cv	cp				
5	0.446429	0.625				

Table A.7: Boundary condidtions for wedge example

*CESE_BOUNDARY_PRESCRIBED_SET					
ssid					
1					
lcid_u	lcid_v	lcid_w	lcid_d	lcid_p	lcid_t
-1					
sf_u	sf_v	sf_w	sf_d	sf_p	sf_t
333.48	47.64	0.0	1.225	1.01325e5	
*CESE_BOUNDARY_NON_REFLECTIVE_SET					
ssid					
2					
4					
5					
*CESE_BOUNDARY_SOLID_WALL_SET					
ssid					
3					

Table A.8: Load curve definitions for wedge example

*DEFINE_CURVE						
lcid	sidr	sfa	sfo	offa	offo	dattyp
1						
a1	o1					
0.0	0.14					
1000000.0	0.14					
*DEFINE_CURVE						
lcid	sidr	sfa	sfo	offa	offo	dattyp
2						
a1	o1					
0.0	0.1583					
1000000.0	0.1583					

Table A.9: Output settings for wedge example

*DATABASE_BINARY_D3PLOT			
dt/cycl	lcdt	beam	npltc
0.5e-4	0		
*INCLUDE			
mesh_ex2.k			
*END			

Table A.10: Control cards for automatic and hexagonal meshing in the tank test

*CESE_CONTROL_SOLVER				
iframe	iflow	igeom		
0	1	3		
*CESE_CONTROL_TIMESTEP				
iddt	cfl	dtint		
2	1.0	1.e-4		
*CESE_CONTROL_LIMITER				
idlmt	alfa	beta	epsr	
0	4.0	1.0	0.0	
*CONTROL_TERMINATION				
endtim	endcyc	dtmin	endeng	endmas
0.02				

Table A.11: Example of one subsection of outlets from the gas generator in the tank test

*include							
lc1u							
*include							
lc1v							
*CESE_BOUNDARY_PRESCRIBED_part							
ssid							
11							
lcid_u	lcid_v	lcid_w	lcid_d	lcid_p	lcid_t		
10111	10112	-1					
sf_u	sf_v	sf_w	sf_d	sf_p	sf_t		
10.0	10.0	0.0	1.251	1.01325e5			
*CESE_BOUNDARY_SOLID_WALL_part							
SURFPRT	LCID	Vx	Vy	Vz	Nx	Ny	Nz
2							
3							
4							
18							

Table A.12: Mesh setup card for automatic meshing in the tank test

*MESH_VOLUME_PART							
1	21	cese					
*MESH_VOLUME							
1							
2	3	4	18	11	22	33	44
55	66						

Table A.13: What needs to be added to have hexagonal meshing in the tank test

*include		
geometry_cese_tank_hexa_block.k		
*CESE_PART		
pid	mid	eosid
100	7	5

Table A.14: What needs to be changed in the control subsection to activate immersed boundary

*CESE_CONTROL_SOLVER				
icese	iflow	igeom	iframe	
200	1	3	0	
*CESE_CONTROL_TIMESTEP				
iddt	cfl	dtint		
2	0.5	1.e-3		
*CESE_CONTROL_LIMITER				
idlmt	alfa	beta	epsr	
0	8.0	1.0	0.0	
0	2.0	1.0	0.5	
*CONTROL_TERMINATION				
endtim	endcyc	dtmin	endeng	endmas
100				